

Symmetries and Asymmetries of $B \rightarrow K^* \mu^+ \mu^-$ Decays in the Standard Model and Beyond

WOLFGANG ALTMANNSHOFER^{*,1}, PATRICIA BALL^{†,1,2}, AOIFE BHARUCHA^{‡,2},
ANDRZEJ J. BURAS^{§,1,3}, DAVID M. STRAUB^{¶,1} AND MICHAEL WICK^{||,1}

¹ *Physik-Department, Technische Universität München, 85748 Garching, Germany*

² *IPPP, Department of Physics, University of Durham, Durham DH1 3LE, UK*

³ *TUM Institute for Advanced Study, Technische Universität München, 80333 München, Germany*

Abstract

The rare decay $B \rightarrow K^*(\rightarrow K\pi)\mu^+\mu^-$ is regarded as one of the crucial channels for B physics as the polarization of the K^* allows a precise angular reconstruction resulting in many observables that offer new important tests of the Standard Model and its extensions. These angular observables can be expressed in terms of CP-conserving and CP-violating quantities which we study in terms of the full form factors calculated from QCD sum rules on the light-cone, including QCD factorization corrections. We investigate all observables in the context of the Standard Model and various New Physics models, in particular the Littlest Higgs model with T-parity and various MSSM scenarios, identifying those observables with small to moderate dependence on hadronic quantities and large impact of New Physics. One important result of our studies is that new CP-violating phases will produce clean signals in CP-violating asymmetries. We also identify a number of correlations between various observables which will allow a clear distinction between different New Physics scenarios.

^{*}wolfgang.altmannshofer@ph.tum.de

[†]Patricia.Ball@durham.ac.uk

[‡]a.k.m.bharucha@durham.ac.uk

[§]andrzej.buras@ph.tum.de

[¶]david.straub@ph.tum.de

^{||}michael.wick@ph.tum.de

1 Introduction

The penguin-induced flavour-changing neutral current (FCNC) transitions $b \rightarrow s$ and $b \rightarrow d$ are among the most valuable probes of flavour physics. They are characterized by their high sensitivity to New Physics (NP) contributions and the particularly large impact of short-distance QCD corrections to the relevant observables like branching ratios and more local quantities, see Ref. [1] for a review. The decay $b \rightarrow s\gamma$ has probably been the most popular FCNC transition ever since its first experimental observation as $B \rightarrow K^*\gamma$ at CLEO in 1993 [2]. Despite its considerable success as benchmark probe, in connection with electroweak precision observables [3], its usefulness is limited by the number of observables it gives access to – the branching ratio and CP asymmetries like the time-dependent CP asymmetry in $B \rightarrow K^*\gamma$ [4].

Much more versatile in this respect is the decay $b \rightarrow s\ell^+\ell^-$ with the possibility to measure, for instance, the differential decay rate in the leptons’ invariant mass. One can also construct asymmetries, like the well-known forward-backward asymmetry (A_{FB}), with differing sensitivity to NP effects. A full angular analysis of $B \rightarrow K^*(\rightarrow K\pi)\ell^+\ell^-$ would give access to a multitude of observables [5]. The downside of such measurements – low statistics – has started to be overcome at the B factories BaBar and Belle, with recent measurements of the forward-backward asymmetry in several bins in the lepton invariant mass and the K^* ’s polarization [6, 7]. Current experimental results are compiled in Tab. 1. The absolute number of events observed is still rather small (230 at Belle [7]), making $B \rightarrow K^*\ell^+\ell^-$ one of the rarest B decays ever observed – at least if the resonance-dominated region around the charmonium resonances with $B \rightarrow K^*\psi(\rightarrow \ell^+\ell^-)$ is excluded. This situation will improve once the LHC experiments have started taking data, allowing one to probe the short-distance physics governing $b \rightarrow s\ell^+\ell^-$ at an unprecedented level of the angular spectrum: a recent study by the LHCb collaboration [10] predicts 7200 signal events (an improvement by an order of magnitude from the present situation) with a data set of 2 fb^{-1} , which corresponds to one nominal year of running.

One difference between the experimental reach of B factories and LHC, though, is the preference of the latter for *exclusive* channels, mainly realized as $B \rightarrow K^*\ell^+\ell^-$. This implies that the analysis of this channel requires control not only over short-distance perturbative effects, described by Wilson coefficients in the relevant effective Hamiltonian, but also long-distance non-perturbative effects, described largely, but not completely, by form factors. It is the objective of our paper to provide such an analysis, based on QCD factorization [11, 12, 13], including a full set of form factors calculated from QCD sum rules on the light-cone [14], and the dominant effects suppressed for large b quark mass. As the LHC has increased sensitivity to charged particles in the final state, we focus on the decays of neutral B ’s,

Experiment	BaBar [8]	Belle [7]	CDF [9]
$\text{BR}(B \rightarrow K^*\mu^+\mu^-) \times 10^7$	$11.1 \pm 1.9 \pm 0.7$	$10.8^{+1.0}_{-1.0} \pm 0.9$	$8.1 \pm 3.0 \pm 1.0$
Number of $B\bar{B}$ events	384×10^6	657×10^6	–

Table 1: Experimental results for the branching ratio of $B \rightarrow K^*\mu^+\mu^-$; the region around the charm resonances with $B \rightarrow K^*\psi(\rightarrow \mu^+\mu^-)$ is excluded. The first error is statistics, the second systematics.

$\bar{B}^0 \rightarrow \bar{K}^{*0}(\rightarrow K^-\pi^+)\mu^+\mu^-$ and its CP-conjugate $B^0 \rightarrow K^{*0}(\rightarrow K^+\pi^-)\mu^+\mu^-$, which have the additional advantage that the flavour of the decaying B meson (B^0 or \bar{B}^0) is unambiguously tagged by the final state. We also focus on $\ell = \mu$ which can be cleanly measured at the LHC; see Ref. [15] for a discussion of $\mu \leftrightarrow e$ effects.

$B \rightarrow K^*\mu^+\mu^-$ decays have been investigated by many authors of whom we can cite only a few. In 1999, Ali et al. calculated the dilepton mass spectrum and A_{FB} in the SM and various SUSY scenarios using naïve factorization and QCD sum rules on the light cone [16]. Later it was shown by Beneke et al. [12, 13] that $B \rightarrow K^*\mu^+\mu^-$ admits a systematic theoretical description using QCD factorization in the heavy quark limit $m_b \rightarrow \infty$. This limit is relevant for small invariant lepton masses and reduces the number of independent form factors from 7 to 2. Spectator effects, neglected in naïve factorization, also become calculable. The drawback is that corrections to that limit are only partially known: for instance, in Ref. [17] power-suppressed effects relevant for isospin asymmetries were calculated.¹ In Ref. [19], a calculation of $B \rightarrow K^*\mu^+\mu^-$ using soft-collinear theory (SCET) was presented. More recently, two analyses appeared which also use QCD factorization and focus on possible NP effects in CP asymmetries [20] and on observables available from angular distributions [21], respectively. There is also vast literature on NP analyses, with varying degrees of reliability of theoretical input for long-distance QCD effects and scope of observables considered. One intrinsic NP contribution, for instance, comes from an extended scalar sector. Most studies available so far, with the notable exception of Ref. [22], focus on the effects of such contributions on A_{FB} , which turn out to be small, while we shall argue that the effect can best be seen in one particular angular observable not considered before, see Sec. 3.

In the present paper, we aim to improve on previous studies in the following way:

- we include the full set of 7 form factors, rather than the 2 form factors in the heavy quark limit, calculated from QCD sum rules on the light-cone; we show that our set of form factors fulfills all correlations required in the heavy quark limit, which has never been demonstrated before for any form factor calculation;
- we give an up-to-date prediction of the $B \rightarrow K^*(\rightarrow K\pi)\mu^+\mu^-$ observables in the SM and shall argue that the bulk of power-suppressed corrections is due to the difference between the full QCD form factors and their heavy quark limit;
- we study all angular observables in the decay $B \rightarrow K^*(\rightarrow K\pi)\mu^+\mu^-$ and identify those with small sensitivity to hadronic and large sensitivity to NP effects;
- we include the effects of scalar and pseudoscalar operators, which are extremely suppressed in the SM, on all angular observables;
- we study the effects of various NP models, including several manifestations of the MSSM and the Littlest Higgs model with T-parity.

Our main results are collected in Sec. 7.

Our paper is organized as follows: in Sec. 2 we review the theoretical framework, based on the trinity of effective Hamiltonian, form factors and QCD factorization. In Sec. 3 we discuss the (rather involved) kinematics of the decay and define the basic observables in the process. Sec. 4 gives a short overview over the NP models whose effects we study. In Sec. 5 we define

¹Very recently, BaBar has reported a positive result [18] for a deviation of the isospin asymmetry from the SM prediction, which so far, however, has not been confirmed by Belle [7].

observables satisfying the requirements of theoretical cleanliness and high sensitivity to NP effects. Section 6, the centre part of our paper, contains the phenomenological analysis of those observables in the SM, in a model-independent way and in several selected NP scenarios. We conclude in Sec. 7. In the appendices we review the kinematics of four-body decays and show that for large b quark mass the form factors calculated, in Sec. 2, from QCD sum rules on the light-cone fulfill the relations imposed by heavy-quark symmetry.

2 Theoretical Framework

The theoretical framework which allows one to calculate the decay amplitude of $B \rightarrow K^* \mu^+ \mu^-$ is quite involved and requires three different steps which are described in this section:

- the separation of short-distance (QCD, weak interaction and new physics) effects from long-distance QCD in an effective Hamiltonian \mathcal{H}_{eff} ;
- the calculation of matrix elements of local quark bilinear operators J of type $\langle K^* | J | B \rangle$ (form factors);
- the calculation of effects of 4-quark operators in \mathcal{H}_{eff} which give rise to so-called non-factorizable corrections and can be calculated using QCD factorization (QCDF).

QCDF is only valid for small invariant dilepton mass $q^2 \sim O(1 \text{ GeV}^2)$, or, equivalently, large K^* energy $E \sim O(m_B/2)$, which implies certain cuts on q^2 or E . In this paper, we restrict ourselves to $1 \text{ GeV}^2 < q^2 < 6 \text{ GeV}^2$. The reasons will be discussed in Sec. 2.4. Obviously, *all* the above steps need to be under good control for a reliable prediction of the decay. We will discuss them in turn and also explain our strategy for calculating the $B \rightarrow K^* \mu^+ \mu^-$ amplitude.

2.1 Effective Hamiltonian

The effective Hamiltonian for $b \rightarrow s \mu^+ \mu^-$ transitions is given by [23, 24]

$$\mathcal{H}_{\text{eff}} = -\frac{4 G_F}{\sqrt{2}} \left(\lambda_t \mathcal{H}_{\text{eff}}^{(t)} + \lambda_u \mathcal{H}_{\text{eff}}^{(u)} \right) \quad (2.1)$$

with the CKM combination $\lambda_i = V_{ib} V_{is}^*$ and

$$\begin{aligned} \mathcal{H}_{\text{eff}}^{(t)} &= C_1 \mathcal{O}_1^c + C_2 \mathcal{O}_2^c + \sum_{i=3}^6 C_i \mathcal{O}_i + \sum_{i=7,8,9,10,P,S} (C_i \mathcal{O}_i + C'_i \mathcal{O}'_i), \\ \mathcal{H}_{\text{eff}}^{(u)} &= C_1 (\mathcal{O}_1^c - \mathcal{O}_1^u) + C_2 (\mathcal{O}_2^c - \mathcal{O}_2^u). \end{aligned}$$

Although the contribution of $\mathcal{H}_{\text{eff}}^{(u)}$ is doubly Cabibbo-suppressed with respect to that of $\mathcal{H}_{\text{eff}}^{(t)}$ and hence often dropped, it proves relevant for certain observables sensitive to complex phases of decay amplitudes, so we keep it. The operators $\mathcal{O}_{i \leq 6}$ are identical to the P_i given in Ref. [23], while the remaining ones are given by

$$\mathcal{O}_7 = \frac{e}{g^2} m_b (\bar{s} \sigma_{\mu\nu} P_R b) F^{\mu\nu}, \quad \mathcal{O}'_7 = \frac{e}{g^2} m_b (\bar{s} \sigma_{\mu\nu} P_L b) F^{\mu\nu}, \quad (2.2)$$

$$\mathcal{O}_8 = \frac{1}{g} m_b (\bar{s} \sigma_{\mu\nu} T^a P_R b) G^{\mu\nu a}, \quad \mathcal{O}'_8 = \frac{1}{g} m_b (\bar{s} \sigma_{\mu\nu} T^a P_L b) G^{\mu\nu a}, \quad (2.3)$$

$$\mathcal{O}_9 = \frac{e^2}{g^2} (\bar{s} \gamma_\mu P_L b) (\bar{\mu} \gamma^\mu \mu), \quad \mathcal{O}'_9 = \frac{e^2}{g^2} (\bar{s} \gamma_\mu P_R b) (\bar{\mu} \gamma^\mu \mu), \quad (2.4)$$

$$\mathcal{O}_{10} = \frac{e^2}{g^2} (\bar{s} \gamma_\mu P_L b) (\bar{\mu} \gamma^\mu \gamma_5 \mu), \quad \mathcal{O}'_{10} = \frac{e^2}{g^2} (\bar{s} \gamma_\mu P_R b) (\bar{\mu} \gamma^\mu \gamma_5 \mu), \quad (2.5)$$

$$\mathcal{O}_S = \frac{e^2}{16\pi^2} m_b (\bar{s} P_R b) (\bar{\mu} \mu), \quad \mathcal{O}'_S = \frac{e^2}{16\pi^2} m_b (\bar{s} P_L b) (\bar{\mu} \mu), \quad (2.6)$$

$$\mathcal{O}_P = \frac{e^2}{16\pi^2} m_b (\bar{s} P_R b) (\bar{\mu} \gamma_5 \mu), \quad \mathcal{O}'_P = \frac{e^2}{16\pi^2} m_b (\bar{s} P_L b) (\bar{\mu} \gamma_5 \mu), \quad (2.7)$$

where g is the strong coupling constant and $P_{L,R} = (1 \mp \gamma_5)/2$. m_b denotes the running b quark mass in the $\overline{\text{MS}}$ scheme. The primed operators with opposite chirality to the unprimed ones vanish or are highly suppressed in the SM, as are $\mathcal{O}_{S,P}$. We neglect the contributions of \mathcal{O}'_i for $1 \leq i \leq 6$. These operators are generated in some NP scenarios, for instance in left-right symmetric models or through gluino contributions in a general MSSM, but their impact is either heavily constrained or turns out to be very small generically.

The Wilson coefficients C_i in (2.1) encode short-distance physics and possible NP effects. They are calculated at the matching scale $\mu = m_W$, in a perturbative expansion in powers of $\alpha_s(m_W)$, and are then evolved down to scales $\mu \sim m_b$ according to the solution of the renormalization group equations. Any NP contributions enter through $C_i(m_W)$, while the evolution to lower scales is determined by the SM. The inclusion of the factors $16\pi^2/g^2 = 4\pi/\alpha_s$ in the definition of the operators $\mathcal{O}_{i \geq 7}$ and the corresponding primed operators serves to allow a more transparent organization of the expansion of their Wilson coefficients in perturbation theory: all C_i are expanded as

$$C_i = C_i^{(0)} + \frac{\alpha_s}{4\pi} C_i^{(1)} + \left(\frac{\alpha_s}{4\pi}\right)^2 C_i^{(2)} + O(\alpha_s^3), \quad (2.8)$$

where $C_i^{(0)}$ is the tree-level contribution, which vanishes for all operators but \mathcal{O}_2 . In our normalization of operators also $C_9^{(0)}$ is non-zero. $C_i^{(n)}$ denotes an n -loop contribution. In our paper we aim at next-to-next-to-leading logarithmic (NNLL) accuracy, which requires the calculation of the matching conditions at $\mu = m_W$ to two-loop accuracy. This has been done in Ref. [23]. NP contributions, on the other hand, will be included to one-loop accuracy only.²

Two-loop accuracy in the matching requires the inclusion of anomalous dimensions in the renormalization-group equations to three-loop accuracy. The corresponding $O(\alpha_s^3)$ entries in the 10×10 SM anomalous dimension matrix have been calculated in Refs. [25, 26]. On the other hand, the operators $\mathcal{O}_{S,P}^{(\prime)}$ are given in terms of conserved currents, i.e. they carry no scale-dependence, they do not mix with other operators and their Wilson coefficients are given by the coefficients at the matching scale. \mathcal{O}_9 is also given by conserved currents, but mixes with $\mathcal{O}_{1,\dots,6}$, via diagrams with a virtual photon decaying into $\mu^+ \mu^-$. Additional scale dependence in C_9 comes from the factor $1/g^2$. The latter dependence is also present in C_{10} , which otherwise would be scale independent.

²An explicit calculation of two-loop corrections in the MSSM [24] shows that they are small.

In Tab. 2 we give all the SM values of the Wilson coefficients to NNLL accuracy. As we shall see below, in Eq. (3.1), $C_{7,9}$ always appear in a particular combination with other C_i in matrix elements. It hence proves convenient to define effective coefficients $C_{7,9}^{(\prime)\text{eff}}$, and also $C_{8,10}^{(\prime)\text{eff}}$, which are given by [29]

$$\begin{aligned}
C_7^{\text{eff}} &= \frac{4\pi}{\alpha_s} C_7 - \frac{1}{3} C_3 - \frac{4}{9} C_4 - \frac{20}{3} C_5 - \frac{80}{9} C_6, \\
C_8^{\text{eff}} &= \frac{4\pi}{\alpha_s} C_8 + C_3 - \frac{1}{6} C_4 + 20 C_5 - \frac{10}{3} C_6, \\
C_9^{\text{eff}} &= \frac{4\pi}{\alpha_s} C_9 + Y(q^2), \\
C_{10}^{\text{eff}} &= \frac{4\pi}{\alpha_s} C_{10}, \quad C_{7,8,9,10}^{\prime\text{eff}} = \frac{4\pi}{\alpha_s} C_{7,8,9,10}', \tag{2.9}
\end{aligned}$$

$$\begin{aligned}
\text{with } Y(q^2) &= h(q^2, m_c) \left(\frac{4}{3} C_1 + C_2 + 6 C_3 + 60 C_5 \right) \\
&\quad - \frac{1}{2} h(q^2, m_b) \left(7 C_3 + \frac{4}{3} C_4 + 76 C_5 + \frac{64}{3} C_6 \right) \\
&\quad - \frac{1}{2} h(q^2, 0) \left(C_3 + \frac{4}{3} C_4 + 16 C_5 + \frac{64}{3} C_6 \right) \\
&\quad + \frac{4}{3} C_3 + \frac{64}{9} C_5 + \frac{64}{27} C_5. \tag{2.10}
\end{aligned}$$

The function

$$h(q^2, m_q) = -\frac{4}{9} \left(\ln \frac{m_q^2}{\mu^2} - \frac{2}{3} - z \right) - \frac{4}{9} (2+z) \sqrt{|z-1|} \times \begin{cases} \arctan \frac{1}{\sqrt{z-1}} & z > 1 \\ \ln \frac{1+\sqrt{1-z}}{\sqrt{z}} - \frac{i\pi}{2} & z \leq 1 \end{cases} \tag{2.11}$$

with $z = 4m_q^2/q^2$, is related to the basic fermion loop.

We shall see below that $B \rightarrow K^*(\rightarrow K\pi)\mu^+\mu^-$ does not allow access to all the above coefficients separately: for instance, only the combinations $C_S - C_S'$ and $C_P - C_P'$ enter the decay amplitude.

2.2 Form Factors

The $B \rightarrow K^*$ matrix elements of the operators $\mathcal{O}_{7,9,10,S,P}^{(\prime)}$ can be expressed in terms of seven form factors which depend on the momentum transfer q^2 between the B and the K^* ($q^\mu = p^\mu - k^\mu$):

$$\langle \bar{K}^*(k) | \bar{s} \gamma_\mu (1 - \gamma_5) b | \bar{B}(p) \rangle = -i \epsilon_\mu^* (m_B + m_{K^*}) A_1(q^2) + i(2p - q)_\mu (\epsilon^* \cdot q) \frac{A_2(q^2)}{m_B + m_{K^*}}$$

$C_1(\mu)$	$C_2(\mu)$	$C_3(\mu)$	$C_4(\mu)$	$C_5(\mu)$	$C_6(\mu)$	$C_7^{\text{eff}}(\mu)$	$C_8^{\text{eff}}(\mu)$	$C_9^{\text{eff}}(\mu) - Y(q^2)$	$C_{10}^{\text{eff}}(\mu)$
-0.257	1.009	-0.005	-0.078	0.000	0.001	-0.304	-0.167	4.211	-4.103
$\bar{C}_1(\mu)$	$\bar{C}_2(\mu)$	$\bar{C}_3(\mu)$	$\bar{C}_4(\mu)$	$\bar{C}_5(\mu)$	$\bar{C}_6(\mu)$	$C_7'^{\text{eff}}(\mu)$	$C_8'^{\text{eff}}(\mu)$		
-0.128	1.052	0.011	-0.032	0.009	-0.037	-0.006	-0.003		

Table 2: SM Wilson coefficients at the scale $\mu = m_b = 4.8 \text{ GeV}$, to NNLL accuracy. All other Wilson coefficients are heavily suppressed in the SM. The “barred” \bar{C}_i are related to C_i as defined in Ref. [12]. Input: $\alpha_s(m_W) = 0.120$, $\alpha_s(m_b) = 0.214$, obtained from $\alpha_s(m_Z) = 0.1176$ [27], using three-loop evolution. We also use $m_t(m_t) = 162.3 \text{ GeV}$ [28], $m_W = 80.4 \text{ GeV}$ and $\sin^2 \theta_W = 0.23$.

$$+ i q_\mu (\epsilon^* \cdot q) \frac{2m_{K^*}}{q^2} [A_3(q^2) - A_0(q^2)] + \epsilon_{\mu\nu\rho\sigma} \epsilon^{*\nu} p^\rho k^\sigma \frac{2V(q^2)}{m_B + m_{K^*}}, \quad (2.12)$$

$$\text{with } A_3(q^2) = \frac{m_B + m_{K^*}}{2m_{K^*}} A_1(q^2) - \frac{m_B - m_{K^*}}{2m_{K^*}} A_2(q^2) \text{ and } A_0(0) = A_3(0); \quad (2.13)$$

$$\begin{aligned} \langle \bar{K}^*(k) | \bar{s} \sigma_{\mu\nu} q^\nu (1 + \gamma_5) b | \bar{B}(p) \rangle &= i \epsilon_{\mu\nu\rho\sigma} \epsilon^{*\nu} p^\rho k^\sigma 2T_1(q^2) \\ &+ T_2(q^2) [\epsilon_\mu^* (m_B^2 - m_{K^*}^2) - (\epsilon^* \cdot q) (2p - q)_\mu] + T_3(q^2) (\epsilon^* \cdot q) \left[q_\mu - \frac{q^2}{m_B^2 - m_{K^*}^2} (2p - q)_\mu \right], \end{aligned} \quad (2.14)$$

with $T_1(0) = T_2(0)$. ϵ_μ is the polarization vector of the K^* . The form factors A_i and V are observables, i.e. scale independent, while the T_i depend on the renormalization scale μ .

A_0 is also the form factor of the pseudoscalar current:

$$\langle \bar{K}^* | \partial_\mu A^\mu | \bar{B} \rangle = (m_b + m_s) \langle \bar{K}^* | \bar{s} i \gamma_5 b | \bar{B} \rangle = 2m_{K^*} (\epsilon^* \cdot q) A_0(q^2). \quad (2.15)$$

The form factors are hadronic quantities and call for a non-perturbative calculation. No lattice calculation of a full set of form factors is available yet. As a recent result we quote a (quenched) value for $T_1(0)$ relevant for $B \rightarrow K^* \gamma$: $T_1(0) = 0.24 \pm 0.03_{-0.01}^{+0.04}$ [30]. Preliminary results from an alternative lattice calculation of $T_1(0)$ have been reported in Ref. [31]. At present, a more promising method for calculating form factors at large energies of the final-state meson (i.e. at small q^2) is offered by QCD sum rules on the light-cone (LCSRs) (s. Ref. [14] for reviews). This method combines standard QCD sum rule techniques with the information on light-cone hadron distribution amplitudes (DAs) familiar from the theory of exclusive processes [32]. It has been applied to $B \rightarrow K^*$ form factors in, for instance, Refs. [33, 34]. The key idea is to consider a correlation function of the $b \rightarrow s$ current and a current with the quantum numbers of the B meson, sandwiched between the vacuum and the K^* . For large (negative) virtualities of these currents, the correlation function is, in coordinate-space, dominated by light-like distances and can be expanded around the light-cone. In contrast to the short-distance expansion employed in conventional QCD sum rules à la Shifman/Vainshtein/Zakharov [35], where non-perturbative effects are encoded in vacuum expectation values of local operators with vacuum quantum numbers, the condensates, LCSRs rely on the factorization of the underlying correlation function into genuinely non-perturbative

and universal hadron DAs ϕ . The DAs are convoluted with process-dependent amplitudes T_H , which similarly to Wilson coefficients can be calculated in perturbation theory, schematically

$$\text{correlation function} \sim \sum_n T_H^{(n)} \otimes \phi^{(n)}. \quad (2.16)$$

The sum runs over contributions with increasing twist, labelled by n , and \otimes means integration over the longitudinal momenta of the partons described by $\phi^{(n)}$. We shall see below that contributions of non-leading twist are suppressed by increasing powers of m_{K^*}/m_b . The same correlation function can, on the other hand, be written as a dispersion-relation, in the virtuality of the current coupling to the B meson. Equating dispersion-representation and light-cone expansion, and separating the B meson contribution from that of higher one- and multi-particle states, one obtains a relation (QCD sum rule) for the form factor.

For $B \rightarrow K^*$ form factors the relevant correlation function is

$$i \int d^4y e^{-ipy} \langle \bar{K}^*(p) | T J_\mu(0) j_B^\dagger(y) | 0 \rangle \propto \Pi(q^2) \quad (2.17)$$

with $j_B = \bar{d}i\gamma_5 b$ and $J_\mu = \bar{s}\gamma_\mu(1 - \gamma_5)b$, $\bar{s}\sigma_{\mu\nu}q^\nu(1 + \gamma_5)b$ or $\bar{s}i\gamma_5 b$. The factor of proportionality contains four-vectors with open indices and/or mass factors like $(m_B + m_{K^*})$ etc., which are irrelevant for dynamics. LCSRs for all 7 form factors except for A_0 are available at $O(\alpha_s)$ accuracy for twist-2 and -3 and tree-level accuracy for twist-4 contributions [34]. For this paper, we have also calculated the LCSR for A_0 to the same accuracy. The correlation function $\Pi(q^2)$, calculated for unphysical p^2 , can be written as dispersion-relation over its physical cut. Singling out the contribution of the B meson, one has, for the pseudoscalar current $J_\mu = \bar{s}i\gamma_5 b$,

$$\Pi(q^2) = A_0(q^2) \frac{m_B^2 f_B}{m_b} \frac{1}{m_B^2 - p^2} + \text{higher poles and cuts}, \quad (2.18)$$

where f_B is the leptonic decay constant of the B meson,

$$f_B m_B^2 = m_b \langle B | \bar{b}i\gamma_5 d | 0 \rangle. \quad (2.19)$$

In the framework of LCSRs one does not use (2.18) as it stands, but performs a Borel-transformation,

$$\hat{B} \frac{1}{t - p^2} = \frac{1}{M^2} \exp(-t/M^2), \quad (2.20)$$

with the Borel-parameter M^2 ; this transformation enhances the ground-state B meson contribution to the dispersion-representation of Π . The next step is to invoke quark-hadron duality to approximate the contributions of hadrons other than the ground-state B meson by the imaginary part of the light-cone expansion of Π , so that

$$\hat{B}\Pi^{\text{LC}} = \frac{1}{M^2} \frac{m_B^2 f_B}{m_b} A_0(q^2) e^{-m_B^2/M^2} + \frac{1}{M^2} \frac{1}{\pi} \int_{s_0}^{\infty} dt \text{Im}\Pi^{\text{LC}}(t) \exp(-t/M^2). \quad (2.21)$$

Subtracting the integral from both sides, Eq. (2.21) becomes the LCSR for A_0 . s_0 is the so-called continuum threshold, which separates the ground-state from the continuum contribution. As with standard QCD sum rules, the use of quark-hadron duality above s_0 and

the choice of s_0 itself introduce a certain model-dependence (or systematic error) in the final result for the form factor.

As an explicit example for a LCSR, we quote the tree-level result for $T_1(0)$ as given in Ref. [36]:

$$\begin{aligned}
\frac{m_B^2 f_B}{m_b} T_1(0) e^{-m_B^2/M^2} &= f_{K^*}^\perp m_b \int_{u_0}^1 du e^{-m_b^2/(uM^2)} \frac{\phi_\perp(u)}{2u} \\
&+ f_{K^*}^\parallel m_{K^*} \int_{u_0}^1 du e^{-m_b^2/(uM^2)} \left[\frac{\Phi(u)}{2u} + \frac{1}{2} g_\perp^{(v)}(u) + \frac{1}{8u} \left(1 - u \frac{d}{du} \right) g_\perp^{(a)}(u) \right. \\
&\quad \left. - \frac{1}{u} \frac{d}{du} \int_0^u d\alpha_1 \int_0^{\bar{u}} d\alpha_2 \frac{u - \alpha_1}{2\alpha_3^2} \left(\mathcal{A}(\underline{\alpha}) + \mathcal{V}(\underline{\alpha}) \right) \right] \\
&+ f_{K^*}^\perp m_b \frac{m_{K^*}^2}{m_b^2} \int_{u_0}^1 du e^{-m_b^2/(uM^2)} \left[\frac{1}{2} \frac{d}{du} \left\{ u \bar{u} \phi_\perp(u) + 2I_L(u) + uH_3(u) \right. \right. \\
&\quad \left. \left. - \int_0^u d\alpha_1 \int_0^{\bar{u}} d\alpha_2 \frac{1}{\alpha_3} \left(S(\underline{\alpha}) - \tilde{S}(\underline{\alpha}) + T_1^{(4)}(\underline{\alpha}) - T_2^{(4)}(\underline{\alpha}) + T_3^{(4)}(\underline{\alpha}) - T_4^{(4)}(\underline{\alpha}) \right) \right\} \right. \\
&\quad \left. - \frac{1}{8} u \frac{d^2}{du^2} \mathbb{A}_\perp(u) \right], \tag{2.22}
\end{aligned}$$

$$\equiv m_b \int_{u_0}^1 du e^{-m_b^2/(uM^2)} \left[f_{K^*}^\perp R_1(u) + f_{K^*}^\parallel \frac{m_{K^*}}{m_b} R_2(u) + f_{K^*}^\perp \left(\frac{m_{K^*}}{m_b} \right)^2 R_3(u) \right], \tag{2.23}$$

where u_0 is given by m_b^2/s_0 . $f_{K^*}^\parallel$ and $f_{K^*}^\perp$ are the decay constants of, respectively, longitudinally and transversely polarized K^* mesons. ϕ_\perp , Φ , $g_\perp^{(v,a)}$, I_L and H_3 are DAs and integrals thereof, as defined in Ref. [34]. \mathcal{A} , \mathcal{V} , S , \tilde{S} and $T_i^{(4)}$ are three-particle DAs. The precise definitions of all these DAs as well as explicit parameterizations can be found in Refs. [37]. In a slight abuse of language, we shall call R_1 the twist-2 contribution to the sum rule, R_2 twist-3 and R_3 twist-4. u is the longitudinal momentum fraction of the quark in a two-particle Fock state of the final-state vector meson, whereas $\alpha_{1,2,3}$, with $\sum \alpha_i = 1$, are the momentum fractions of the partons in a three-particle state. The light-cone expansion is accurate up to terms of order $(m_{K^*}/m_b)^3$. Up-to-date results for these DAs can be found in Ref. [37]. Although we only write down the tree-level expression for the form factor, radiative corrections are known for R_1 [33] and the two-particle contributions to R_2 [34], and will be included in the numerical analysis. All scale-dependent quantities are calculated at the (infra-red) factorization scale $\mu_F^2 = m_B^2 - m_b^2$. The form factor itself carries an ultra-violet scale dependence. As a default, we choose $\mu = m_b$ for that ultra-violet scale.

It is clearly visible from the above formula that the respective weight of various contributions is controlled by the parameter m_{K^*}/m_b ; the next term in the light-cone expansion contains twist-3, -4 and -5 DAs and is of order $(m_{K^*}/m_b)^3$. Numerically, the expansion works very well, with the $O(m_{K^*}^2/m_b^2)$ terms contributing less than 5% to the LCSRs. Note that the expansion is in m_{K^*}/m_b only for $q^2 = 0$. For $q^2 > 0$, the expansion parameter is, see App. B, $m_b m_{K^*}/(m_b^2 - q^2) \approx m_{K^*}/(2E)$, E being the energy of the K^* . Obviously, the smaller E

B parameters			
f_B [39]	$\lambda_B(\mu_h)$ [36]	μ_h	
200(25) MeV	0.51(12) GeV	2.2 GeV	
K^* parameters			
$f_{K^*}^{\parallel}$	$f_{K^*}^{\perp}(2\text{GeV})$	$a_1^{\perp,\parallel}(2\text{GeV})$	$a_2^{\perp,\parallel}(2\text{GeV})$
220(5) MeV	163(8) MeV	0.03(3)	0.08(6)
quark masses			
$m_b(m_b)$ [40]	$m_c(m_c)$ [40]	$m_t(m_t)$ [28]	
4.20(4) GeV	1.30(2) GeV	162.3(1.1) GeV	

Table 3: Numerical values of hadronic input parameters. $a_i^{\perp,\parallel}$ are parameters of the twist-2 K^* DAs and are taken from Ref. [37], from where we also take all higher-twist parameters not included in the table.

(and the larger q^2), the more relevant the higher-twist terms. For $E \rightarrow m_{K^*}$, the light-cone expansion breaks down.

The LCSR method sketched above does not rely on m_b being a large (or hard) scale – LCSRs also work very well for D meson decays, see Ref. [38]. In order to calculate the $B \rightarrow K^* \mu^+ \mu^-$ decay amplitude, however, knowing the form factors is not enough: there are additional terms which can be calculated using QCD factorization, see the next subsection.

As for numerics, we collect the most important input parameters in Tab. 3. We evaluate the sum rules at $M^2 = 8 \text{ GeV}^2$ and choose s_0 such that the minimum in M^2 is at 8 GeV^2 . The resulting s_0 lie all between 33 GeV^2 and 37 GeV^2 . Note that the LCSR return results for f_B times the form factor, rather than the form factor itself. Hence the LCSR must be divided by f_B which, as one can see from Tab. 3, comes with a rather large error. It is well known that the resulting prediction for, for instance, $T_1(0)$ is on the high side compared with the experimental result that can be extracted from the branching ratio of $B \rightarrow K^* \gamma$, assuming the absence of New Physics [12]. For this reason we *fix* the value of f_B to reproduce the experimental value $T_1^{\text{exp}}(0) = 0.268$ [41]. This corresponds to setting $f_B = 0.186 \text{ GeV}$ – well within the allowed range quoted in Tab. 3. As the observables we calculate are ratios, the normalization and the precise value of f_B cancel in the end – which is why we neglect the residual experimental and theoretical error of $T_1^{\text{exp}}(0)$ and f_B of about 7% [41]. The resulting values of the form factors at $q^2 = 0$ are given in Tab. 4. With f_B fixed, the errors of the form factors become rather small and are below 20%.

As for the q^2 -dependence, it follows directly from the sum rules. In Fig. 1 we plot the central values of all form factors as functions of q^2 .

2.3 QCD Factorization

In addition to terms proportional to the form factors, the $B \rightarrow K^* \mu^+ \mu^-$ amplitude also contains certain “non-factorizable” effects that do not correspond to form factors. They are related to matrix elements of the purely hadronic operators \mathcal{O}_1 to \mathcal{O}_6 and the chromomagnetic-dipole operator \mathcal{O}_8 with additional (virtual) photon emission. These effects can, in the com-

$A_0(0)$	$A_1(0)$	$A_2(0)$	$V(0)$
0.333 ± 0.033	0.233 ± 0.038	0.190 ± 0.039	0.311 ± 0.037
$T_1(0)$	$T_3(0)$	$\xi_{\parallel}(0)$	$\xi_{\perp}(0)$
0.268 ± 0.045	0.162 ± 0.023	0.118 ± 0.008	0.266 ± 0.032

Table 4: LCSR results for $q^2 = 0$. $T_2(0) = T_1(0)$. The scale-dependent form factors T_i and $\xi_{\parallel,\perp}$ are evaluated at $\mu = 4.8 \text{ GeV}$. The soft form factors $\xi_{\perp,\parallel}$ are introduced in Sec. 2.3. The error is calculated from varying s_0 by $\pm 2 \text{ GeV}^2$, M^2 by $\pm 2 \text{ GeV}^2$ and all hadronic input parameters according to their uncertainties given in Tab. 3, except for f_B , see text.

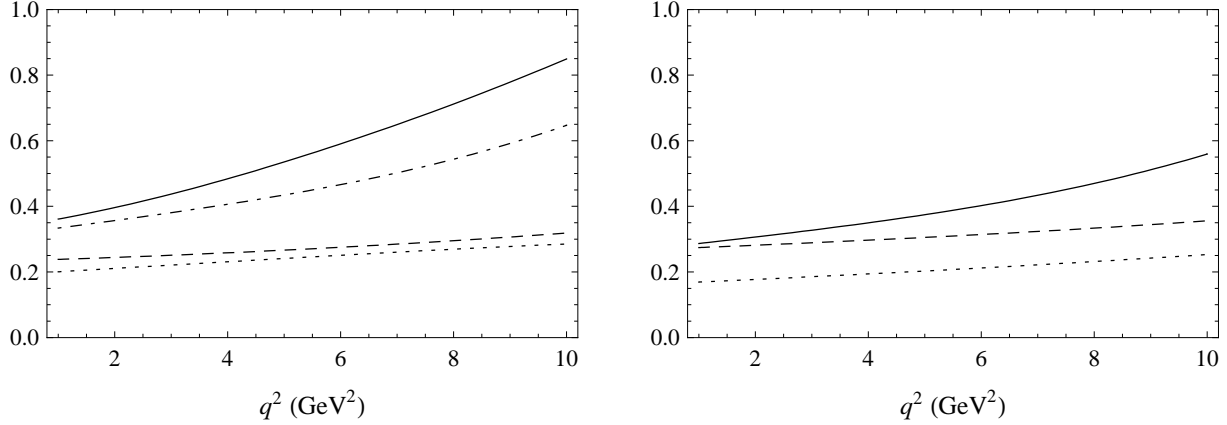


Figure 1: Form factors from LCSRs for central values of input parameters. Left: Solid curve: A_0 , long dashes: A_1 , short dashes: A_2 , dot-dashed curve: V . Right: Solid curve: T_1 , long dashes: T_2 , short dashes: T_3 .

bined heavy quark and large energy limit, be calculated using QCD factorization (QCDF) methods [11, 12, 13]. Here large energy means large energy of the K^* , $E \sim O(m_B/2)$. E is related to q^2 , the dilepton mass, by

$$2m_B E = m_B^2 + m_{K^*}^2 - q^2. \quad (2.24)$$

For the phenomenological analysis in later sections, we require $E > 2.1 \text{ GeV}$, which corresponds to $q^2 < 6 \text{ GeV}^2$, well below the charm threshold. We would like to stress here that QCDF *does not work* for large q^2 above the charm resonances – here the only theoretical prediction we have are the contributions to the $B \rightarrow K^* \mu^+ \mu^-$ matrix element given in terms of the form factors, which is probably a reasonable approximation at the 10 to 20% level.

In the heavy quark and large energy limit, the number of independent form factors reduces from 7 to 2 which correspond to the polarization of the K^* (transversal or longitudinal) and are usually denoted by ξ_{\perp} and ξ_{\parallel} . Neglecting for the moment $O(\alpha_s)$ corrections, one can define the ξ 's as [13]

$$\xi_{\perp}(q^2) = \frac{m_B}{m_B + m_{K^*}} V(q^2), \quad (2.25)$$

$$\xi_{\parallel}(q^2) = \frac{m_B + m_{K^*}}{2E} A_1(q^2) - \frac{m_B - m_{K^*}}{m_B} A_2(q^2). \quad (2.26)$$

At this point we would like to recall that the large energy limit is also familiar from the description of hard perturbative QCD processes à la Brodsky-Lepage [42]. For instance, the electromagnetic form factor of the π can be factorized into a convolution of the DAs of the initial and final state pion and a perturbative hard scattering amplitude, schematically

$$F_\pi(Q^2) \sim \phi_\pi \otimes T_H \otimes \phi_\pi. \quad (2.27)$$

As in the previous subsection, the \otimes stands for integration of the longitudinal momenta of all hard partons in the process. Note that T_H is due to hard-gluon exchange between the π constituents and hence is $O(\alpha_s)$. In this “hard mechanism” only valence-quark configurations contribute and all quarks have large longitudinal momentum. The subtlety with heavy meson decays, however, is that the power-counting of various contributions in $1/m_b$ differs from that of the π EM form factor and similar processes, and that a second mechanism contributes at the same (leading) order in $1/m_b$. This is the so-called soft or Feynman mechanism, where not all partons in the meson participate in the hard subprocess; it involves highly asymmetric configurations where the spectator quark stays soft, but the light quark produced in the weak decay has large energy. This mechanism is described by the ξ form factors, which, as a consequence, are also called soft form factors, and the factorization formula for $B \rightarrow K^*$ decay form factors reads, schematically:

$$F(q^2) = D\xi(E) + \phi_B \otimes T_H \otimes \phi_{K^*} + O(1/m_b), \quad (2.28)$$

where $D = 1 + O(\alpha_s)$ includes hard corrections to the weak vertex and E is the energy of the K^* . As made explicit by the last term on the right-hand side, the above formula is not exact, but will receive corrections (both soft and hard) which are suppressed by powers of m_b . These corrections are unknown to date. An additional complication is that the separation between the “soft” contributions included in the form factor ξ and the “hard” contributions in the convolution is not clear-cut and requires the definition of a factorization scheme [11]. In Ref. [13], the factorization scheme is defined by (2.25) and (2.26), absorbing the hard and hard-spectator corrections into the definition of the ξ ’s. Eqs. (2.25) and (2.26) are then valid to all orders in α_s . The redundancy of 5 form factors in the heavy quark limit induces a number of relations between them. We discuss these relations, and test their validity at finite b quark mass, in App. B.

Coming back to the non-factorizable corrections to $B \rightarrow K^* \mu^+ \mu^-$ mentioned before, it turns out that they can be included in a factorization formula very similar to that for form factors: apart from overall factors and the Lorentz structure, the relevant terms in the decay amplitude can be written as [13]

$$\mathcal{T}_a^{(i)} = \xi_a C_a^{(i)} + \phi_B \otimes T_a^{(i)} \otimes \phi_{a,K^*} + O(1/m_b), \quad (2.29)$$

with $a = \perp, \parallel$ and $i = u, t$. Note that the $C_a^{(i)}$ in the above formula are *not* Wilson coefficients. They do, however, contain both factorizable corrections related to the rewriting of the full QCD form factors by the ξ ’s using (2.28) and non-factorizable corrections related to the matrix elements of hadronic operators with virtual photon emission. Also note that $\mathcal{O}_{7,9,10}$ only contain a 2-quark operator and hence do not induce non-factorizable corrections.

2.4 Our Strategy

Based on the above discussion, our strategy for calculating $B \rightarrow K^*(\rightarrow K\pi)\mu^+\mu^-$ decays is the following:

- we predict observables in the dilepton mass range $1 \text{ GeV}^2 < q^2 < 6 \text{ GeV}^2$;
- we include the main source of power-suppressed corrections by using the full QCD form factors in the naïvely factorized amplitude, and the ξ form factors in the QCDF corrections;
- we concentrate on the prediction of observables which are independent of the absolute values of form factors, and only depend on their ratios;
- for the error analysis, we employ the correlated errors between form factors, which follow from the light-cone sum rules;
- we include new-physics effects in the Wilson coefficients $C_{7,9,10,S,P}$, and their primed counterparts, but not in the other C_i .

A few comments are in order. Obviously QCDF breaks down close to the charm resonances. Technically, this shows up as a threshold at $q^2 = 4m_c^2$. In order to stay sufficiently below the threshold, we set $q_{\text{max}}^2 = 6 \text{ GeV}^2$. On the other hand, for small q^2 close to the kinematical minimum, the decay amplitude is dominated by the photon pole and by just one Wilson coefficient, C_7^{eff} . Hence, by probing the region of very small q^2 , one does not get any new information as compared to the well-studied radiative decay $b \rightarrow s\gamma$. In addition, as the photon virtuality is small, there could be (unknown) resonance contributions from ρ or other mesons. In order to avoid this region, we set $q_{\text{min}}^2 = 1 \text{ GeV}^2$.

As for power-suppressed corrections, we view QCDF as an expansion in two small parameters, $1/m_b$ and α_s and restrict ourselves to the first order in these parameters. While $O(\alpha_s)$ corrections are completely covered by QCDF, those in $1/m_b$ are not included. One source of such corrections are obviously the differences between the 7 full QCD form factors and the 2 soft form factors ξ . Since the light-cone sum rules allow a calculation of all 7 form factors, all these corrections are included in our calculation. An obvious question, though, is whether these are *all* α_s^0/m_b corrections or not. As we shall see in Sec. 3.4, one QCDF correction to naïve factorization is weak annihilation, where the quarks in the B meson annihilate. This contribution is of leading order in $1/m_b$, with unknown power-suppressed corrections. For the decay processes we consider, this contribution comes with small Wilson coefficients, so the impact of $1/m_b$ corrections is negligible. Another potential source of $1/m_b$ corrections are such with formal α_s/m_b counting, but an end-point divergence in the convolution integral. Such divergent integrals were found in power-suppressed corrections relevant for isospin violation [17]. They signal the breakdown of QCDF and call for soft contributions to mend the divergence. Such soft contributions involve soft gluons and hence α_s is not to be evaluated at a hard scale, but becomes non-perturbative, thus rendering this contribution $O(1/m_b)$ in our counting. While it is not known how to calculate such contributions in the context of QCDF, similar contributions do occur in light-cone sum rules and are described by three-particle distribution amplitudes of type $\langle 0 | \bar{q} G s | \bar{K}^* \rangle$, with G the gluonic field-strength tensor. Although these contributions could, *a priori*, be large due to soft-gluon effects, it turns out that such three-particle couplings are numerically small [37] and that, as mentioned in Sec. 2.2, their contribution to form factors is negligible. Based on this, we do not expect any sizeable effects of such terms at $O(1/m_b)$ and conclude that the main source of power-suppressed corrections are those from form factors.

3 Differential Decay Distribution and Spin Amplitudes

In this section we discuss the kinematics of the 4-body decay $B \rightarrow K^*(\rightarrow K\pi)\mu^+\mu^-$, define the angular observables in the spectrum and derive explicit formulas in terms of form factors and Wilson coefficients.

3.1 Differential Decay Distribution

The actual decay being observed in experiment is not $B \rightarrow K^*\mu^+\mu^-$, but $B \rightarrow K^*(\rightarrow K\pi)\mu^+\mu^-$. As discussed in Ref. [5], the additional information provided by the angle between K and π is sensitive to the polarization of the K^* and thus provides an additional probe of the effective Hamiltonian.

The matrix element of the effective Hamiltonian (2.1) for the decay $B \rightarrow K^*(\rightarrow K\pi)\mu^+\mu^-$ can be written, in naïve factorization, as

$$\begin{aligned} \mathcal{M} = & \frac{G_F \alpha}{\sqrt{2}\pi} V_{tb} V_{ts}^* \left\{ \left[\langle K\pi | \bar{s} \gamma^\mu (C_9^{\text{eff}} P_L + C_9'^{\text{eff}} P_R) b | \bar{B} \rangle \right. \right. \\ & - \frac{2m_b}{q^2} \langle K\pi | \bar{s} i \sigma^{\mu\nu} q_\nu (C_7^{\text{eff}} P_R + C_7'^{\text{eff}} P_L) b | \bar{B} \rangle \left. \right] (\bar{\mu} \gamma_\mu \mu) \\ & + \langle K\pi | \bar{s} \gamma^\mu (C_{10}^{\text{eff}} P_L + C_{10}'^{\text{eff}} P_R) b | \bar{B} \rangle (\bar{\mu} \gamma_\mu \gamma_5 \mu) \\ & \left. + \langle K\pi | \bar{s} (C_S P_R + C_S' P_L) b | \bar{B} \rangle (\bar{\mu} \mu) + \langle K\pi | \bar{s} (C_P P_R + C_P' P_L) b | \bar{B} \rangle (\bar{\mu} \gamma_5 \mu) \right\}. \end{aligned} \quad (3.1)$$

To express the $B \rightarrow K\pi$ matrix elements in terms of the $B \rightarrow K^*$ form factors discussed in Sec. 2.2, one assumes that the K^* decays resonantly. Then, one can use a narrow-width approximation by making the following replacement in the squared K^* propagator:

$$\frac{1}{(k^2 - m_{K^*}^2)^2 + (m_{K^*} \Gamma_{K^*})^2} \xrightarrow{\Gamma_{K^*} \ll m_{K^*}} \frac{\pi}{m_{K^*} \Gamma_{K^*}} \delta(k^2 - m_{K^*}^2). \quad (3.2)$$

In this way, the form factors are independent of the $K^* K \pi$ coupling $g_{K^* K \pi}$ [5, 43], because it cancels between the vertex factor and the width

$$\Gamma_{K^*} = \frac{g_{K^* K \pi}^2}{48\pi} m_{K^*} \beta^3, \quad (3.3)$$

where

$$\beta = \frac{1}{m_{K^*}^2} [m_{K^*}^4 + m_K^4 + m_\pi^4 - 2(m_{K^*}^2 m_K^2 + m_K^2 m_\pi^2 + m_{K^*}^2 m_\pi^2)]^{1/2}. \quad (3.4)$$

Writing the matrix elements in Sec. 2.2 as

$$\langle \bar{K}^*(k) | J_\mu | \bar{B}(p) \rangle = \epsilon^{*\nu} A_{\nu\mu}, \quad (3.5)$$

where $A_{\nu\mu}$ contains the $B \rightarrow K^*$ form factors, the corresponding $B \rightarrow K\pi$ matrix element can then be expressed as

$$\langle \bar{K}(k_1) \pi(k_2) | J_\mu | \bar{B}(p) \rangle = -D_{K^*}(k^2) W^\nu A_{\nu\mu}, \quad (3.6)$$

where [5]

$$|D_{K^*}(k^2)|^2 = g_{K^*K\pi}^2 \frac{\pi}{m_{K^*}\Gamma_{K^*}} \delta(k^2 - m_{K^*}^2) = \frac{48\pi^2}{\beta^3 m_{K^*}^2} \delta(k^2 - m_{K^*}^2), \quad (3.7)$$

$$W^\mu = K^\mu - \frac{m_K^2 - m_\pi^2}{k^2} k^\mu, \quad k^\mu = k_1^\mu + k_2^\mu, \quad K^\mu = k_1^\mu - k_2^\mu. \quad (3.8)$$

With an on-shell K^* , the decay is completely described by four independent kinematical variables: the dilepton invariant mass squared q^2 and the three angles θ_{K^*} , θ_l and ϕ as defined in App. A. Squaring the matrix element, summing over spins of the final state particles and making use of the kinematical identities sketched in App. A, one obtains the full angular decay distribution of $\bar{B}^0 \rightarrow \bar{K}^{*0}(\rightarrow K^-\pi^+)\mu^+\mu^-$:

$$\frac{d^4\Gamma}{dq^2 d\cos\theta_l d\cos\theta_{K^*} d\phi} = \frac{9}{32\pi} I(q^2, \theta_l, \theta_{K^*}, \phi), \quad (3.9)$$

where

$$\begin{aligned} I(q^2, \theta_l, \theta_{K^*}, \phi) = & I_1^s \sin^2 \theta_{K^*} + I_1^c \cos^2 \theta_{K^*} + (I_2^s \sin^2 \theta_{K^*} + I_2^c \cos^2 \theta_{K^*}) \cos 2\theta_l \\ & + I_3 \sin^2 \theta_{K^*} \sin^2 \theta_l \cos 2\phi + I_4 \sin 2\theta_{K^*} \sin 2\theta_l \cos \phi \\ & + I_5 \sin 2\theta_{K^*} \sin \theta_l \cos \phi \\ & + (I_6^s \sin^2 \theta_{K^*} + I_6^c \cos^2 \theta_{K^*}) \cos \theta_l + I_7 \sin 2\theta_{K^*} \sin \theta_l \sin \phi \\ & + I_8 \sin 2\theta_{K^*} \sin 2\theta_l \sin \phi + I_9 \sin^2 \theta_{K^*} \sin^2 \theta_l \sin 2\phi. \end{aligned} \quad (3.10)$$

The corresponding expression for the CP-conjugated mode $B^0 \rightarrow K^{*0}(\rightarrow K^+\pi^-)\mu^+\mu^-$ is

$$\frac{d^4\bar{\Gamma}}{dq^2 d\cos\theta_l d\cos\theta_{K^*} d\phi} = \frac{9}{32\pi} \bar{I}(q^2, \theta_l, \theta_{K^*}, \phi). \quad (3.11)$$

The function $\bar{I}(q^2, \theta_l, \theta_{K^*}, \phi)$ is obtained from (3.10) by the replacements [5]

$$I_{1,2,3,4,7}^{(a)} \longrightarrow \bar{I}_{1,2,3,4,7}^{(a)}, \quad I_{5,6,8,9}^{(a)} \longrightarrow -\bar{I}_{5,6,8,9}^{(a)}, \quad (3.12)$$

where $\bar{I}_i^{(a)}$ equals $I_i^{(a)}$ with all weak phases conjugated. The minus sign in (3.12) is a result of our convention that, while θ_{K^*} is the angle between the \bar{K}^{*0} and the K^- flight direction or between the K^{*0} and the K^+ , respectively, the angle θ_l is measured between the \bar{K}^{*0} (K^{*0}) and the lepton μ^- in *both* modes. Thus, a CP transformation interchanging lepton and antilepton leads to the transformations $\theta_l \rightarrow \theta_l - \pi$ and $\phi \rightarrow -\phi$, as can be seen from Eqs. (A.1) and (A.2). This convention agrees with Refs. [5, 20, 44], but is different from the convention used in some experimental publications [10], where θ_l is defined as the angle between K^{*0} and μ^+ in the B^0 decay, but between \bar{K}^{*0} and μ^- in the \bar{B}^0 decay.

The angular coefficients $I_i^{(a)}$, which are functions of q^2 only, are usually expressed in terms of \bar{K}^* transversity amplitudes. Since we want to explicitly keep lepton-mass effects and include also contributions from scalar and pseudoscalar operators, this step deserves a closer look.

3.2 Transversity Amplitudes

To introduce the transversity amplitudes, consider for the moment the decay $B \rightarrow K^* V^*$, with the B meson decaying to an on-shell K^* and a virtual photon or Z boson (which can later decay into a lepton-antilepton pair). The amplitude for this process can be written as

$$\mathcal{M}_{(m,n)}(B \rightarrow K^* V^*) = \epsilon_{K^*}^{*\mu}(m) M_{\mu\nu} \epsilon_{V^*}^{*\nu}(n) \quad (3.13)$$

where $\epsilon_{V^*}^\mu(n)$ is the polarization vector of the virtual gauge boson, which can be transverse ($n = \pm$), longitudinal ($n = 0$) or timelike ($n = t$). In the B meson rest frame, the four basis vectors can be written as [43, 45]

$$\epsilon_{V^*}^\mu(\pm) = (0, 1, \mp i, 0)/\sqrt{2}, \quad (3.14)$$

$$\epsilon_{V^*}^\mu(0) = (-q_z, 0, 0, -q_0)/\sqrt{q^2}, \quad (3.15)$$

$$\epsilon_{V^*}^\mu(t) = (q_0, 0, 0, q_z)/\sqrt{q^2}, \quad (3.16)$$

where $q^\mu = (q_0, 0, 0, q_z)$ is the four-momentum vector of the gauge boson. They satisfy the orthonormality and completeness relations

$$\epsilon_{V^*}^{*\mu}(n) \epsilon_{V^* \mu}(n') = g_{nn'}, \quad (3.17)$$

$$\sum_{n,n'} \epsilon_{V^*}^{*\mu}(n) \epsilon_{V^*}^\nu(n') g_{nn'} = g^{\mu\nu}, \quad (3.18)$$

where $n, n' = t, \pm, 0$ and $g_{nn'} = \text{diag}(+, -, -, -)$.

The K^* , on the other hand, is on shell and thus has only three polarization states, $\epsilon_{K^*}^\mu(m)$ with $m = \pm, 0$, which read in the B rest frame

$$\epsilon_{K^*}^\mu(\pm) = (0, 1, \pm i, 0)/\sqrt{2}, \quad (3.19)$$

$$\epsilon_{K^*}^\mu(0) = (k_z, 0, 0, k_0)/m_{K^*}, \quad (3.20)$$

where $k^\mu = (k_0, 0, 0, k_z)$ is the four-momentum vector of the K^* (note that $k_z = -q_z$). They satisfy the relations

$$\epsilon_{K^*}^{*\mu}(m) \epsilon_{K^* \mu}(m') = -\delta_{mm'}, \quad (3.21)$$

$$\sum_{m,m'} \epsilon_{K^*}^{*\mu}(m) \epsilon_{K^*}^\nu(m') \delta_{mm'} = -g^{\mu\nu} + \frac{k^\mu k^\nu}{m_{K^*}^2}. \quad (3.22)$$

The helicity amplitudes H_0 , H_+ and H_- can now be projected out from $M_{\mu\nu}$ by contracting with the explicit polarization vectors in (3.13),

$$H_m = \mathcal{M}_{(m,m)}(B \rightarrow K^* V^*), \quad m = 0, +, -. \quad (3.23)$$

Alternatively, one can work with the transversity amplitudes defined as [44]

$$A_{\perp,\parallel} = (H_{+1} \mp H_{-1})/\sqrt{2}, \quad A_0 \equiv H_0. \quad (3.24)$$

In contrast to the decay of B to two (on-shell) vector mesons, to which this formalism can also be applied, there is an additional transversity amplitude in the case of $B \rightarrow K^* V^*$ because the gauge boson is virtual, namely

$$A_t = \mathcal{M}_{(0,t)}(B \rightarrow K^* V^*), \quad (3.25)$$

which corresponds to a K^* polarization vector which is longitudinal in the K^* rest frame and a V^* polarization vector which is timelike in the V^* rest frame.³

If we now consider the subsequent decay of the gauge boson into a lepton-antilepton pair, the amplitude becomes

$$\mathcal{M}(B \rightarrow K^* V^*(\rightarrow \mu^+ \mu^-))(m) \propto \epsilon_{K^*}^{*\mu}(m) M_{\mu\nu} \sum_{n,n'} \epsilon_{V^*}^{*\nu}(n) \epsilon_{V^*}^\rho(n') g_{nn'} (\bar{\mu} \gamma_\rho P_{L,R} \mu). \quad (3.26)$$

This amplitude can now be expressed in terms of six transversity amplitudes $A_{\perp,\parallel,0}^L$ and $A_{\perp,\parallel,0}^R$, where L and R refer to the chirality of the leptonic current, as well as the seventh transversity amplitude A_t . The reason that for A_t no separate left-handed and right-handed parts have to be considered can be seen as follows. Noticing that the timelike polarization vector in (3.16) is simply given by $\epsilon_{V^*}^\mu(t) = q^\mu / \sqrt{q^2}$, one can see from current conservation,

$$q^\mu (\bar{\mu} \gamma^\mu \mu) = 0, \quad q^\mu (\bar{\mu} \gamma^\mu \gamma_5 \mu) = 2im_\mu (\bar{\mu} \gamma_5 \mu), \quad (3.27)$$

that the timelike component of the V^* can only couple to an axial-vector current. In addition, this shows that A_t vanishes in the limit of massless leptons.

Now, having shown that the amplitude of the sequential decay $B \rightarrow K^* V^*(\rightarrow \mu^+ \mu^-)$ can be expressed in terms of seven transversity amplitudes, it is clear that this is true for all contributions of the operators $\mathcal{O}_7^{(\prime)}$, $\mathcal{O}_9^{(\prime)}$ and $\mathcal{O}_{10}^{(\prime)}$ to the decay of interest, $B \rightarrow K^*(\rightarrow K\pi)\mu^+\mu^-$, regardless of whether they originate from virtual gauge boson exchange (i.e. photon or Z penguin diagrams) or from box diagrams.

Does this also apply to decays mediated not by a vector, but a scalar and pseudoscalar operator? Inspecting Eqs. (2.6), (2.7) and (3.27), one can see that the combination $(\mathcal{O}_P - \mathcal{O}_P')$ can be absorbed into the transversity amplitude A_t , because it couples to axial-vector currents, just like the timelike component of a virtual gauge boson. However, this is not possible for the scalar operators $\mathcal{O}_S^{(\prime)}$. Therefore, the inclusion of scalar operators in the decay $B \rightarrow K^*(\rightarrow K\pi)\mu^+\mu^-$ requires the introduction of an additional, “scalar” transversity amplitude, which we denote A_S .

To summarize, the treatment of the decay $B \rightarrow K^*(\rightarrow K\pi)\mu^+\mu^-$ by decomposition of the amplitude into seven transversity amplitudes $A_{\perp,\parallel,0}^{L,R}$ and A_t is sufficient as long as the operators $\mathcal{O}_{7,9,10}^{(\prime)}$ and $\mathcal{O}_P^{(\prime)}$ are considered, but has to be supplemented by an additional, eighth transversity amplitude A_S once contributions from scalar operators are taken into account.

Finally, we give the explicit form of the eight transversity amplitudes (up to corrections of $O(\alpha_s)$, whose discussion we postpone until Sec. 3.4):

$$A_{\perp,L,R} = N\sqrt{2}\lambda^{1/2} \left[[(C_9^{\text{eff}} + C_9^{\text{eff}\prime}) \mp (C_{10}^{\text{eff}} + C_{10}^{\text{eff}\prime})] \frac{V(q^2)}{m_B + m_{K^*}} + \frac{2m_b}{q^2} (C_7^{\text{eff}} + C_7^{\text{eff}\prime}) T_1(q^2) \right], \quad (3.28)$$

³Unlike sometimes stated in the literature, A_t does not correspond to a timelike polarization of the K^* meson. As mentioned above, the K^* decays on the mass shell and thus has only three polarization states.

$$A_{\parallel L,R} = -N\sqrt{2}(m_B^2 - m_{K^*}^2) \left[[(C_9^{\text{eff}} - C_9^{\text{eff}'}) \mp (C_{10}^{\text{eff}} - C_{10}^{\text{eff}'})] \frac{A_1(q^2)}{m_B - m_{K^*}} + \frac{2m_b}{q^2}(C_7^{\text{eff}} - C_7^{\text{eff}'})T_2(q^2) \right], \quad (3.29)$$

$$A_{0L,R} = -\frac{N}{2m_{K^*}\sqrt{q^2}} \left\{ [(C_9^{\text{eff}} - C_9^{\text{eff}'}) \mp (C_{10}^{\text{eff}} - C_{10}^{\text{eff}'})] \times \left[(m_B^2 - m_{K^*}^2 - q^2)(m_B + m_{K^*})A_1(q^2) - \lambda \frac{A_2(q^2)}{m_B + m_{K^*}} \right] + 2m_b(C_7^{\text{eff}} - C_7^{\text{eff}'}) \left[(m_B^2 + 3m_{K^*}^2 - q^2)T_2(q^2) - \frac{\lambda}{m_B^2 - m_{K^*}^2}T_3(q^2) \right] \right\}, \quad (3.30)$$

$$A_t = \frac{N}{\sqrt{q^2}} \lambda^{1/2} \left[2(C_{10}^{\text{eff}} - C_{10}^{\text{eff}'}) + \frac{q^2}{2m_\mu}(C_P - C'_P) \right] A_0(q^2), \quad (3.31)$$

$$A_S = -N\lambda^{1/2}(C_S - C'_S)A_0(q^2), \quad (3.32)$$

where

$$N = V_{tb}V_{ts}^* \left[\frac{G_F^2 \alpha^2}{3 \cdot 2^{10} \pi^5 m_B^3} q^2 \lambda^{1/2} \beta_\mu \right]^{1/2}, \quad (3.33)$$

with $\lambda = m_B^4 + m_{K^*}^4 + q^4 - 2(m_B^2 m_{K^*}^2 + m_{K^*}^2 q^2 + m_B^2 q^2)$ and $\beta_\mu = \sqrt{1 - 4m_\mu^2/q^2}$.

3.3 Angular Coefficients

With the eight transversity amplitudes defined in the preceding subsection, the angular coefficients I_i in (3.10) can be written as

$$I_1^s = \frac{(2 + \beta_\mu^2)}{4} [|A_\perp^L|^2 + |A_\parallel^L|^2 + (L \rightarrow R)] + \frac{4m_\mu^2}{q^2} \text{Re}(A_\perp^L A_\perp^{R*} + A_\parallel^L A_\parallel^{R*}), \quad (3.34)$$

$$I_1^c = |A_0^L|^2 + |A_0^R|^2 + \frac{4m_\mu^2}{q^2} [|A_t|^2 + 2\text{Re}(A_0^L A_0^{R*})] + \beta_\mu^2 |A_S|^2, \quad (3.35)$$

$$I_2^s = \frac{\beta_\mu^2}{4} [|A_\perp^L|^2 + |A_\parallel^L|^2 + (L \rightarrow R)], \quad (3.36)$$

$$I_2^c = -\beta_\mu^2 [|A_0^L|^2 + (L \rightarrow R)], \quad (3.37)$$

$$I_3 = \frac{1}{2} \beta_\mu^2 [|A_\perp^L|^2 - |A_\parallel^L|^2 + (L \rightarrow R)], \quad (3.38)$$

$$I_4 = \frac{1}{\sqrt{2}} \beta_\mu^2 [\text{Re}(A_0^L A_\parallel^{L*}) + (L \rightarrow R)], \quad (3.39)$$

$$I_5 = \sqrt{2}\beta_\mu \left[\text{Re}(A_0^L A_\perp^{L*}) - (L \rightarrow R) - \frac{m_\mu}{\sqrt{q^2}} \text{Re}(A_\parallel^L A_S^* + A_\parallel^R A_S^*) \right], \quad (3.40)$$

$$I_6^s = 2\beta_\mu [\text{Re}(A_\parallel^L A_\perp^{L*}) - (L \rightarrow R)], \quad (3.41)$$

$$I_6^c = 4\beta_\mu \frac{m_\mu}{\sqrt{q^2}} \text{Re} [A_0^L A_S^* + (L \rightarrow R)], \quad (3.42)$$

$$I_7 = \sqrt{2}\beta_\mu \left[\text{Im}(A_0^L A_\parallel^{L*}) - (L \rightarrow R) + \frac{m_\mu}{\sqrt{q^2}} \text{Im}(A_\perp^L A_S^* + A_\perp^R A_S^*) \right], \quad (3.43)$$

$$I_8 = \frac{1}{\sqrt{2}}\beta_\mu^2 [\text{Im}(A_0^L A_\perp^{L*}) + (L \rightarrow R)], \quad (3.44)$$

$$I_9 = \beta_\mu^2 [\text{Im}(A_\parallel^{L*} A_\perp^L) + (L \rightarrow R)]. \quad (3.45)$$

A few comments are in order:

- In contrast to the transversity amplitudes themselves, the angular coefficients I_i are all physical observables. In fact, they contain the complete information that can be extracted from the measurement of the decay $\bar{B}^0 \rightarrow \bar{K}^{*0}(\rightarrow K^-\pi^+)\mu^+\mu^-$. We will discuss in Sec. 5 which combinations of the angular coefficients constitute *theoretically clean* observables.
- In the limit of massless leptons, the well-known relations $I_1^s = 3I_2^s$ and $I_1^c = -I_2^c$ hold.
- The coefficient I_6^c vanishes unless contributions from scalar operators *and* lepton mass effects are taken into account. Therefore, to our knowledge, it has never been considered in the literature before. However, it is a potentially good observable for scalar currents. We will come back to this point in Sec. 6.2.3.

3.4 Additional Corrections to Transversity Amplitudes

As mentioned in Sec. 3.2, the transversity amplitudes (3.28) to (3.32) do not include effects from spectator interactions, which do induce, on the one hand, $O(\alpha_s)$ corrections and, on the other hand, corrections from weak annihilation (WA). These corrections have been calculated within the QCD factorization (QCDF) framework in Refs. [12] and [13] in terms of the soft form factors ξ_\perp and ξ_\parallel discussed in Sec. 2.3.

In Ref. [12], there are two types of $O(\alpha_s)$ corrections, factorizable and non-factorizable. The factorizable corrections arise when expressing the full form factors in terms of ξ_\parallel and ξ_\perp , are given by the radiative corrections in Eqs. (B.1)–(B.4) and therefore are redundant in our set-up. The only exception arises upon expressing the running b quark mass in the operators $\mathcal{O}_{7,8}$, Eqs. (2.2) and (2.3), by a mass parameter in a different renormalization scheme. In the numerical analysis, however, we use the running b quark mass in the $\overline{\text{MS}}$ scheme, so all factorizable $O(\alpha_s)$ corrections calculated in Refs. [12, 13] have to be dropped.

The second QCDF correction to the transversity amplitude in Sec. 3.2 is given by the WA contribution, $T_{\parallel,-}^{(0)}(u, \omega)$ in the notation of Ref. [12]. It is induced by the penguin operators \mathcal{O}_3 and \mathcal{O}_4 and hence is numerically small, see Tab. 2. This is a term which is leading in $1/m_b$

and $O(\alpha_s)$, so in principle one should also include power-suppressed and radiative corrections. However, in view of its small size, we feel justified in neglecting them. As discussed in Ref. [13], there are further WA corrections which are suppressed by one power of m_b with respect to the leading terms. For the leading CKM amplitude in λ_t , see Eq. (2.1), these are again due to penguin-annihilation diagrams and hence can be neglected due to the smallness of the Wilson coefficients. The WA contribution to the λ_u amplitude vanishes for $B^0 \rightarrow K^{*0}\mu^+\mu^-$, but contains, for $B^+ \rightarrow K^{*+}\mu^+\mu^-$, the factor $C_2 \approx 1$ and hence should be included for this process. As, in this work, however, we focus on neutral B meson decays, we can neglect all WA contributions except for $T_{\parallel,-}^{(0)}(u, \omega)$.

On introducing the chirality-flipped operators, the $\mathcal{T}_{\perp,\parallel}^{(t,u)}$ introduced in Sec. 2.3 are promoted to $\mathcal{T}_{\perp,\parallel}^{\pm(t,u)}$ corresponding to the notations of Ref. [46]. In terms of these quantities, we can define the additional corrections to the transversity amplitudes⁴:

$$\begin{aligned}\Delta A_{\perp L,R}^{\text{QCDF}} &= \sqrt{2}N \frac{2m_b}{q^2} (m_B^2 - q^2) (\mathcal{T}_{\perp}^{+(t),\text{WA}+\text{nf}} + \hat{\lambda}_u \mathcal{T}_{\perp}^{+(u)}), \\ \Delta A_{\parallel L,R}^{\text{QCDF}} &= -\sqrt{2}N \frac{2m_b}{q^2} (m_B^2 - q^2) (\mathcal{T}_{\perp}^{-(t),\text{WA}+\text{nf}} + \hat{\lambda}_u \mathcal{T}_{\perp}^{-(u)}), \\ \Delta A_{0L,R}^{\text{QCDF}} &= \frac{N(m_B^2 - q^2)^2}{m_{K^*} m_B^2 \sqrt{q^2}} m_b (\mathcal{T}_{\parallel}^{-(t),\text{WA}+\text{nf}} + \hat{\lambda}_u \mathcal{T}_{\parallel}^{-(u)}).\end{aligned}\tag{3.46}$$

The superscript, WA+nf, on $\mathcal{T}_{\perp}^{\pm(t)}$ indicates that only contributions from WA and non-factorizable $O(\alpha_s)$ corrections are to be included. In accordance with Ref. [20], we define $\hat{\lambda}_u = \lambda_u/\lambda_t$. The total transversity amplitudes are given by the expressions in (3.28)–(3.30) plus the above terms ΔA^{QCDF} . Note there are no corrections to A_t or A_S .

4 Testing the SM and its Extensions

4.1 Preliminaries

The multitude of observables accessible in $B \rightarrow K^*\mu^+\mu^-$ decays allows one to test the SM and its extensions more locally than is possible through global quantities like branching ratios and the dimuon mass spectrum. The goal of this section is to describe very briefly the extensions of the SM that we will analyse numerically in Sec. 6. To this end we distinguish different classes of models using two properties:

- the presence or absence of additional operators in the effective weak Hamiltonian relative to the SM ones,
- the presence or absence of new sources of flavour and CP violation beyond the CKM matrix.

When appropriate, we will also comment on the correlation between observables in $B \rightarrow K^*\mu^+\mu^-$ and other important observables in B physics, such as the mass difference in the

⁴It should be noted that the functions $F_{1,2,u}^{(7,9)}$ entering the non-factorizable corrections are defined with a different overall sign in Refs. [13] and [47].

neutral $B_{d,s}$ meson systems, $\Delta M_{d,s}$, and the time-dependent CP asymmetries S in various decay channels. These are: $S_{\psi K_S}$, measured in $B_d \rightarrow J/\psi K_S$, which in the SM equals $\sin 2\beta$, β being one of the angles of the unitarity triangle; $S_{\phi K_S}$, originating from the $b \rightarrow s\bar{s}s$ penguin-decay $B_d \rightarrow \phi K_S$, which in the SM also equals $\sin 2\beta$, but is sensitive to new CP-violating phases in $b \rightarrow s$ transitions; $S_{\psi\phi}$, measured in $B_s \rightarrow J/\psi\phi$, given by the B_s mixing phase, which in the SM is close to zero.⁵

First, however, we would like to stress the importance of the observables in $B \rightarrow K^*(\rightarrow K\pi)\mu^+\mu^-$ for tests of the SM.

4.2 Standard Model

The importance of the observables discussed in the present paper for tests of the SM originates from the following facts:

- Several of the observables we consider are predicted to be strongly suppressed in the SM or even vanish so that New Physics (NP) effects can be seen more easily than in the branching ratio of $B \rightarrow K^*\mu^+\mu^-$ which is measured to be consistent with the SM expectations.
- The relatively small number of relevant SM parameters which are already well constrained by a number of processes allows rather definitive predictions for many observables subject mainly to the theoretical uncertainty of form factors.
- In certain cases the sign of a given observable has a unique prediction in the SM, which can be tested more easily than the magnitude itself.

However, to use these facts in a meaningful way, it is essential to have reliable calculations of the relevant form factors. In fact the use of the improved form factors presented in our paper and the consideration of correlations between the uncertainties of the different form factors allows one to obtain rather reliable predictions for angular coefficients in the SM.

4.3 Models with Minimal Flavour Violation (MFV)

The simplest class of extensions of the SM are models with constrained MFV (CMFV) in which the operators are SM-like, all flavour violating transitions are governed by the CKM matrix and also CP-violating observables are SM-like [49, 50, 51]. NP effects in this class of models affect the Wilson coefficients at the scale $O(m_W)$ and collect NP contributions from scales higher than m_W . At the same time, the QCD renormalization group evolution down to scales lower than m_W is universal for all CMFV models and the same as in the SM. It can be shown that this class of models is characterized by strong correlations between observables in B_d , B_s and K processes [50].

The implications of these correlations and of the fact that all flavour violating interactions are governed by the CKM matrix are striking: deviations from the SM predictions for most weak-decay observables are bounded to be at most 50%, often much less [52, 53]. Moreover, the predictions for CP asymmetries are generically identical to the SM ones. Consequently, the distinction between various models of this class on the basis of global quantities like branching ratios is very challenging. We will investigate whether more local quantities like

⁵There are, however, hints from the Tevatron that this phase might actually be large [48].

the angular observables considered in our paper could be helpful in this respect. Obviously any measurement of a non-standard CP-asymmetry would immediately signal new sources of CP violation beyond the CMFV framework.

The symmetry-based definition of MFV [54] does not exclude the appearance of additional non-SM operators. Compared to the CMFV framework, large effects can be expected in particular from scalar operators. The most popular model in this respect is the MFV MSSM which boasts an extensive literature. In this model the CKM matrix remains the only source of flavour and CP violation, but, in particular at large $\tan\beta$, additional scalar and/or pseudoscalar operators, not present in CMFV models, enter the game. For instance in $B_{s,d} \rightarrow \mu^+\mu^-$ decays the presence of such scalar or pseudoscalar operators which are induced by Higgs penguin diagrams can enhance the branching ratio by one order of magnitude with respect to the SM, models with CMFV and the Littlest Higgs model with T parity.

The discovery of $B_s \rightarrow \mu^+\mu^-$ with a branching ratio of $O(10^{-8})$ would be a clear signal of non-standard scalar or pseudoscalar operators. In Sec. 6 we shall demonstrate that it is precisely the angular observables in $B \rightarrow K^*(\rightarrow K\pi)\mu^+\mu^-$ that allow one to distinguish whether scalar or pseudoscalar currents would be responsible for such an enhancement.

4.4 Flavour-Blind MSSM

As a modest, but interesting modification of the MSSM with MFV we consider the so-called Flavour Blind MSSM (FBMSSM) [55, 56, 57, 58]. In this framework, the CKM matrix remains the only source of flavour violation, while new flavour conserving, but CP-violating phases are present in the soft sector. To be more specific, we assume universal soft masses for the different squark flavours and flavour-diagonal trilinear couplings at the electroweak scale, allowing for complex values of the latter parameters.

One would naïvely expect that CP-violating, but flavour conserving observables, such as electric dipole moments (EDMs), would be the best probes by far for CP violation in the FBMSSM. However, it turns out that large new CP-violating effects in flavour physics can still occur at an experimentally visible level. In particular, there is still a lot of room for CP-violating asymmetries in B decays, like $A_{CP}(b \rightarrow s\gamma)$ and $S_{\phi_{KS}}$, while $S_{\psi\phi}$ is well constrained.

The dipole operators play the most relevant role in this context and, as shown in Ref. [58], striking correlations between electric dipole moments of neutron and electron, the $S_{\phi_{KS}}$ asymmetry and $A_{CP}(b \rightarrow s\gamma)$ are present in this model. In particular this framework links the explanation of the suppression of $S_{\phi_{KS}}$ relative to $S_{\psi_{KS}}$, measured at the B factories, to a large enhancement of $A_{CP}(b \rightarrow s\gamma)$ and the EDMs of the neutron and the electron, $d_{n,e}$, over their SM values.

Therefore it is of interest to investigate whether the addition of flavour conserving, but CP-violating phases in the soft sector would have a visible impact on $B \rightarrow K^*(\rightarrow K\pi)\mu^+\mu^-$ and consequently whether the FBMSSM could also be tested with the help of the observables discussed in the present paper. As we will see below, very interesting and predictive results are in fact obtained in this framework.

4.5 Littlest Higgs Model with T-Parity (LHT)

Another class of models of interest are those in which the operators remain as in the SM, but new sources of both flavour and CP violation beyond the CKM matrix are present. In

this class of models the CMFV correlations between B_d , B_s and K observables are generally violated and much larger NP effects than in CMFV models are possible.

A prominent example of this class of models is the Littlest Higgs model with T-parity [59, 60] in which the interactions between SM quarks and heavy mirror quarks, mediated by new heavy charged and neutral gauge bosons, involve a new mixing matrix that differs from the CKM matrix [61] and is parameterized by three new mixing angles and three new CP-violating phases [62].

A number of detailed analyses of FCNC processes in the LHT model has shown that large departures from SM predictions for FCNC processes are still possible in this model while satisfying all existing constraints [63, 64, 65, 66]. In particular the CP asymmetry $S_{\psi\phi}$ can be enhanced by an order of magnitude relative to the SM prediction [63, 67] which would be welcome if the data from the Tevatron [48] will be confirmed by more accurate measurements at LHCb. We will investigate whether the LHT model can also be tested efficiently by means of the angular observables in $B \rightarrow K^*(\rightarrow K\pi)\mu^+\mu^-$. All loop functions with mirror quarks and new heavy weak-boson exchanges have been calculated in Refs. [63, 64]. A very recent paper, Ref. [66], finds additional contributions to Z penguin relative to Ref. [64]. We will investigate the importance of these terms in our analysis.

4.6 General MSSM

Finally we also consider the MSSM with generic flavour- and CP-violating soft SUSY-breaking terms. In such a framework one is confronted with a large number of free parameters which make it very difficult to perform global analyses.

The flavour-mixing off-diagonal entries in the squark mass matrices, usually called mass insertions, present in this framework can lead to complex contributions to the Wilson coefficients of all operators in Eqs. (2.2) to (2.7). On the other hand, the mass insertions are not completely free parameters, but are constrained by measurements of many FCNC processes like $\text{BR}(B \rightarrow X_s\gamma)$, $\text{BR}(B \rightarrow X_s\mu^+\mu^-)$, ΔM_s , ΔM_d , $S_{\psi K_S}$ and others [68, 69, 70, 71]. The remaining parameter space still allows sizeable effects in the Wilson coefficients governing $B \rightarrow K^*\mu^+\mu^-$. The general MSSM contributions to these Wilson coefficients have been studied for both inclusive decays, $B \rightarrow X_s\mu^+\mu^-$ [72, 73], and exclusive channels, $B \rightarrow K^{(*)}\mu^+\mu^-$ [46, 74]. In Sec. 6.3.4 we investigate the possible impact of these contributions on the observables discussed in the following Sec. 5, focusing in particular on the question of how to distinguish the general MSSM framework from the other models described above.

5 Observables

As discussed in Sec. 3, the decay $\bar{B}^0 \rightarrow \bar{K}^{*0}(\rightarrow K^-\pi^+)\mu^+\mu^-$ is completely described in terms of twelve angular coefficient functions $I_i^{(a)}$. The corresponding CP-conjugate mode $B^0 \rightarrow K^{*0}(\rightarrow K^+\pi^-)\mu^+\mu^-$ gives access to twelve additional observables, the CP-conjugate angular coefficient functions $\bar{I}_i^{(a)}$. These quantities have a clear relation to both experiment and theory: theoretically they are expressed in terms of transversity amplitudes, and experimentally they describe the angular distribution. A physical interpretation of these $I_i^{(a)}$ can be drawn from Eqs. (3.34) to (3.45). For example, I_6^c depends on scalar operators and I_7 to I_9 depend on the imaginary part of the transversity amplitudes, and consequently on their phases, which come

	$m_\mu = 0$	$m_\mu \neq 0$
SM	18	22
SM + $\mathcal{O}_S^{(f)}$	20	24

Table 5: Number of independent observables in $B \rightarrow K^*(\rightarrow K\pi)\mu^+\mu^-$, depending on whether lepton mass effects and/or scalar operators are taken into account.

either from QCD effects and enter the QCD factorisation expressions at $O(\alpha_s)$, see Sec. 2, or are CP-violating SM or NP phases.

To separate CP-conserving and CP-violating NP effects, we find it more convenient to consider the twelve CP averaged angular coefficients

$$S_i^{(a)} = \left(I_i^{(a)} + \bar{I}_i^{(a)} \right) \bigg/ \frac{d(\Gamma + \bar{\Gamma})}{dq^2} \quad (5.1)$$

as well as the twelve CP asymmetries⁶

$$A_i^{(a)} = \left(I_i^{(a)} - \bar{I}_i^{(a)} \right) \bigg/ \frac{d(\Gamma + \bar{\Gamma})}{dq^2}. \quad (5.2)$$

These are our primary observables that will be used in the phenomenological analysis in Sec. 6. They offer a clean and comprehensive way to analyse the full richness of angular distributions in $B \rightarrow K^*(\rightarrow K\pi)\mu^+\mu^-$ decays. We shall show below that all previously studied observables, for example the forward-backward asymmetry A_{FB} , can be easily expressed in terms of our new observables. $S_i^{(a)}$ and $A_i^{(a)}$ are normalized to the CP-averaged dilepton mass distribution to reduce both experimental and theoretical uncertainties. Taking the CP average means that CP-violating effects in the $S_i^{(a)}$ are washed out, resulting in a cleaner observable. Taking the CP asymmetry, on the other hand, means that any non-standard CP violation can be easily identified.

These CP asymmetries, i.e. $A_i^{(a)}$, are expected to be small in the SM, as previously noted in Ref. [20]. This is because the only CP-violating phase affecting the decay enters via λ_u in Eq. (2.1) and is doubly Cabibbo-suppressed. Therefore we are particularly keen to examine these asymmetries in the context of CP-violating phases in NP models.

It should be stressed that out of these 24 observables, two vanish in the SM, namely S_6^c and A_6^c , which are generated only by scalar operators, and four are related in the limit of massless leptons through $S_1^s = 3S_2^s$, $S_1^c = -S_2^c$ and $A_1^s = 3A_2^s$, $A_1^c = -A_2^c$ (see Sec. 3.3). Table 5 summarizes the number of independent observables in these limits.

In addition, even for non-zero lepton mass, only three of the four $S_{1,2}^{s,c}$ are independent, which can be seen as follows. The dilepton mass distribution can be expressed in terms of angular coefficients as

$$\frac{d\Gamma}{dq^2} = \frac{3}{4}(2 I_1^s + I_1^c) - \frac{1}{4}(2 I_2^s + I_2^c). \quad (5.3)$$

Therefore, due to the normalization (5.1), there is the relation

$$\frac{3}{4}(2 S_1^s + S_1^c) - \frac{1}{4}(2 S_2^s + S_2^c) = 1. \quad (5.4)$$

⁶ Note that our definition of the CP asymmetries differs from Ref. [20] by a factor of $\frac{3}{2}$.

Consequently, the complete set of 24 independent observables would be given by the twelve $A_i^{(a)}$, eleven $S_i^{(a)}$ and the CP-averaged dilepton mass distribution $d(\Gamma + \bar{\Gamma})/dq^2$. However, the latter is the only observable for which the normalization of the form factors is relevant, so theoretically it is not as clean.

In our opinion, the quantities $S_i^{(a)}$ and $A_i^{(a)}$ are the natural starting point for an experimental analysis. In Ref. [21], a detailed investigation was carried out showing that a full angular fit was the preferred way to extract observables. This would involve fitting Eqs. (3.9) and (3.11) to data. From such a fit the $I_i^{(a)}$ and $\bar{I}_i^{(a)}$ would be found directly, and could be combined using Eqs. (5.1) and (5.2) to give the desired quantities. We suggest that a similar full angular fit could be carried out for the four-fold spectrum $d^4(\Gamma \pm \bar{\Gamma})$, so $S_i^{(a)}$ and $A_i^{(a)}$ would be instantly accessible. Note that, due to Eq. (3.12), the CP-averaged decay distribution $d^4(\Gamma + \bar{\Gamma})$ gives access to $S_{1,2,3,4,7}^{(a)}$ and $A_{5,6,8,9}^{(a)}$, while the remaining observables can be obtained from $d^4(\Gamma - \bar{\Gamma})$.

Alternatively, $S_i^{(a)}$ and $A_i^{(a)}$ can be found by taking asymmetries and/or integrating $d^4(\Gamma \pm \bar{\Gamma})$ over the angles θ_l , θ_K and ϕ . Details for the extraction of some of the $A_i^{(a)}$ are given in Ref. [20], but we stress that all our observables can be determined in a similar manner. To illustrate this point, one case not mentioned in Ref. [20] is S_5 , which can be obtained by integrating over two angles:

$$S_5 = -\frac{4}{3} \left[\int_{\pi/2}^{3\pi/2} - \int_0^{\pi/2} - \int_{3\pi/2}^{2\pi} \right] d\phi \left[\int_0^1 - \int_{-1}^0 \right] d \cos \theta_K \frac{d^3(\Gamma - \bar{\Gamma})}{dq^2 d \cos \theta_K d\phi} \bigg/ \frac{d(\Gamma + \bar{\Gamma})}{dq^2}. \quad (5.5)$$

As stated above, we normalize the $S_i^{(a)}$ and $A_i^{(a)}$ to the CP-averaged dilepton mass distribution in order to reduce the dependence on the form factors. Our approach described in Secs. 3.2 and 3.4 makes use of the full form factors for the dominant leading-order contribution and the soft form factors for additional suppressed contributions. Therefore our results are largely independent of the relation between the soft form factors and the full form factors. However, to further our understanding of these soft form factor relations, we investigate them and their q^2 dependence in App. B. It is found that relations involving ξ_\perp are almost independent of q^2 , whereas those involving ξ_\parallel have a considerable dependence on q^2 due to the neglected $1/m_b$ terms. Therefore we stress that the transversity amplitudes $A_{\perp,\parallel}^{L,R}$ of Sec. 3.2, and all angular observables built from them, should be more or less insensitive to $1/m_b$ corrections, i.e. corrections to QCDF, while $A_0^{L,R}$ and all corresponding angular variables will be slightly more affected by such corrections. These findings impact on prior work carried out in this channel, where the transversity amplitudes were given entirely in terms of the soft form factors using QCDF.

All established observables can be expressed in terms of $S_i^{(a)}$ and $A_i^{(a)}$. For example, the CP asymmetry in the dilepton mass distribution is given by (see Eq. (5.4))

$$A_{\text{CP}} = \frac{d(\Gamma - \bar{\Gamma})}{dq^2} \bigg/ \frac{d(\Gamma + \bar{\Gamma})}{dq^2} = \frac{3}{4} (2 A_1^s + A_1^c) - \frac{1}{4} (2 A_2^s + A_2^c). \quad (5.6)$$

We prefer to define the normalized forward-backward asymmetry as a ratio of CP-averaged quantities, to wit

$$A_{\text{FB}} = \left[\int_0^1 - \int_{-1}^0 \right] d \cos \theta_l \frac{d^2(\Gamma - \bar{\Gamma})}{dq^2 d \cos \theta_l} \bigg/ \frac{d(\Gamma + \bar{\Gamma})}{dq^2} = \frac{3}{8} (2 S_6^s + S_6^c). \quad (5.7)$$

The CP average is numerically irrelevant in the SM, but makes the connection to experiment more transparent. In addition, this definition is complementary to the forward-backward CP asymmetry [75],

$$A_{\text{FB}}^{\text{CP}} = \left[\int_0^1 - \int_{-1}^0 \right] d \cos \theta_l \frac{d^2(\Gamma + \bar{\Gamma})}{dq^2 d \cos \theta_l} \bigg/ \frac{d(\Gamma + \bar{\Gamma})}{dq^2} = \frac{3}{8} (2 A_6^s + A_6^c). \quad (5.8)$$

Additional well-established observables are the K^* longitudinal and transverse polarization fractions F_L , F_T , which are usually defined in terms of transversity amplitudes. We prefer to directly express them in terms of CP-averaged observables and *define*

$$F_L = -S_2^c, \quad F_T = 4S_2^s. \quad (5.9)$$

The well-known relation $F_T = 1 - F_L$ is then a consequence of Eq. (5.4) in the limit of vanishing lepton mass.

In Refs. [44, 21], the transverse asymmetries $A_T^{(i)}$ were introduced. They can be expressed in terms of our observables as

$$\begin{aligned} A_T^{(2)} &= \frac{S_3}{2 S_2^s}, \\ A_T^{(3)} &= \left(\frac{4 S_4^2 + S_7^2}{-2 S_2^c (2 S_2^s + S_3)} \right)^{1/2}, \\ A_T^{(4)} &= \left(\frac{S_5^2 + 4 S_8^2}{4 S_4^2 + S_7^2} \right)^{1/2}. \end{aligned} \quad (5.10)$$

Finally, for some observables it is useful to consider their q^2 average. We define

$$\langle S_i^{(a)} \rangle = \int_{1 \text{ GeV}^2}^{6 \text{ GeV}^2} dq^2 \left(I_i^{(a)} + \bar{I}_i^{(a)} \right) \bigg/ \int_{1 \text{ GeV}^2}^{6 \text{ GeV}^2} dq^2 \frac{d(\Gamma + \bar{\Gamma})}{dq^2}, \quad (5.11)$$

$$\langle A_i^{(a)} \rangle = \int_{1 \text{ GeV}^2}^{6 \text{ GeV}^2} dq^2 \left(I_i^{(a)} - \bar{I}_i^{(a)} \right) \bigg/ \int_{1 \text{ GeV}^2}^{6 \text{ GeV}^2} dq^2 \frac{d(\Gamma + \bar{\Gamma})}{dq^2}. \quad (5.12)$$

The reasons for choosing the interval $1 \text{ GeV}^2 \leq q^2 \leq 6 \text{ GeV}^2$ are discussed in Sec. 2.4.

We proceed in the next section by studying the predictions for $S_i^{(a)}$ and $A_i^{(a)}$, keeping in mind the sensitivity to hadronic effects. This is carried out first in the SM and later in the various NP models described in Sec. 4.

6 Phenomenological Analysis

We are now in a position to perform a phenomenological analysis of the observables defined in Sec. 5, first in the SM, then in a model-independent manner, and finally for specific NP scenarios.

6.1 Standard Model

Our predictions for the CP-averaged angular coefficients $S_i^{(a)}$ in the SM are shown in Fig. 2. S_1^s and S_1^c have been omitted since the relations $S_1^s = 3S_2^s$ and $S_1^c = -S_2^c$ (see Sec. 3.3) are fulfilled up to lepton-mass effects, which amount to at most 1%. $S_{1,2}^{s,c}$ are numerically large as expected. S_4, S_5, S_6^s are similar in magnitude, but are particularly interesting as they each have a zero in q^2 . All these predictions are seen to have small uncertainties, as the normalization results in a cancellation of hadronic effects. In Tab. 6, we show our predictions for the positions of the zeros of S_4, S_5 and S_6^s , denoted by $q_0^2(S_i)$ from now on. S_3 is numerically small in the SM since it is approximately proportional to the chirality-flipped Wilson coefficient C_7'' , which is suppressed by a factor m_s/m_b . S_7, S_8 and S_9 are small as well and have a larger error-band as they arise from the imaginary part of the transversity amplitudes.

The error bands have been obtained by adding various uncertainties in quadrature. We estimate the uncertainty due to the form factors by varying the Borel parameter and continuum threshold as discussed in Sec. 2.2. The renormalization-scale uncertainty is found by varying μ between 4.0 and 5.6 GeV, where μ is the scale at which the Wilson coefficients, α_s and the $\overline{\text{MS}}$ masses are evaluated. We also include parametric uncertainties which are estimated by varying the hadronic parameters as indicated in Tab. 3, the ratio m_c/m_b between 0.25 and 0.33, and the CKM angle γ , which is particularly important for the doubly Cabibbo-suppressed contribution to the CP asymmetries, between 60° and 80° .⁷ In addition, we show the leading-order prediction as a dashed line. We find that the impact of radiative QCDF corrections is moderate for observables like $S_{2,3,4,5,6}$ that, in the SM, are largely independent of weak or strong phases, but becomes more prominent for observables built from imaginary parts, like $S_{7,8,9}$ and A_i , where the main contribution comes from strong phases induced by $O(\alpha_s)$ corrections in QCDF.

Some of these $S_i^{(a)}$ can be directly compared to previous results in the literature. S_2^s and S_2^c correspond to the K^* longitudinal and transverse polarization fractions F_L and F_T , see Eq. (5.9), and S_6^s yields the forward-backward asymmetry A_{FB} , see Eq. (5.7). In particular, $q_0^2(S_6^s)$ in Tab. 6 is identical to the zero of the forward-backward asymmetry which has been extensively studied in the literature. For completeness, in the last row of Fig. 2 we also show the CP averaged dilepton mass distribution $d(\Gamma + \bar{\Gamma})/dq^2$ and the observables $A_T^{(3)}$ and $A_T^{(4)}$ defined in Ref. [21], see Sec. 5. We find that our results for all these observables compare well to those in the literature. However, we note that the peak in the plot of $A_T^{(4)}$ is a manifestation of the zero $q_0^2(S_4)$ of S_4 , see Eq. (5.10). This division by a near-zero quantity induces a large theoretical uncertainty both in the position of the peak and its height. We stress that such uncertainties do not arise if the observables S_4 and S_5 are considered instead of $A_T^{(3)}$ and $A_T^{(4)}$. In fact, as $d\Gamma/dq^2$ is a smooth function in the range of q^2 considered, none of our observables S_i and A_i is affected by accidental and delicate cancellations in the denominator.

⁷The discontinuity in some of the error bands just below 6 GeV² is an unphysical artifact resulting from small charm quark masses ~ 1.2 GeV allowed in the estimation of the error. This feature was already observed in Ref. [12].

Obs.	S_4	S_5	S_6^s
$q_0^2 [\text{GeV}^2]$	$1.94^{+0.12}_{-0.10}$	$2.24^{+0.06}_{-0.08}$	$3.90^{+0.11}_{-0.12}$

Table 6: Predictions for the zero positions $q_0^2(S_i)$ of S_4, S_5 and S_6^s in the SM.

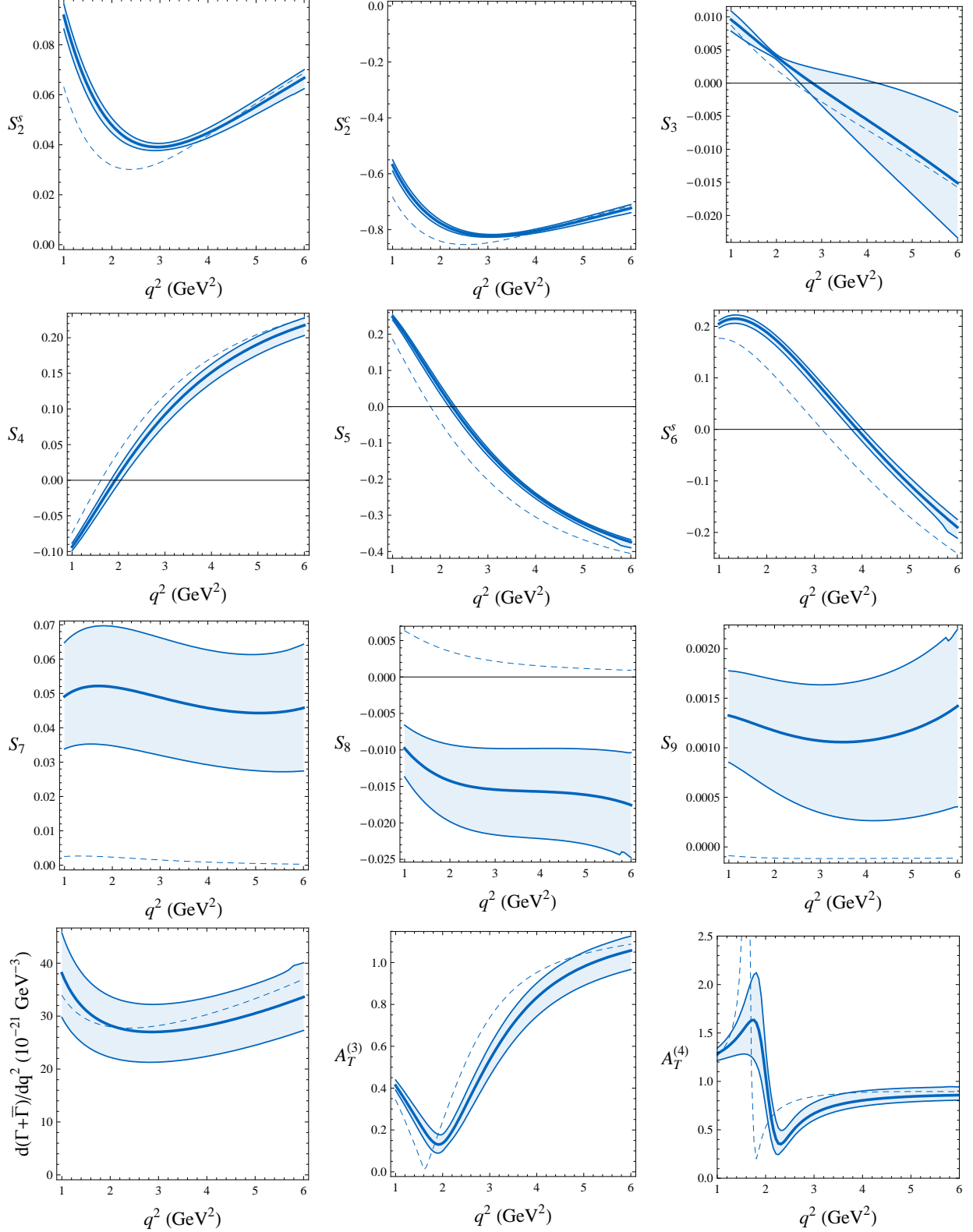


Figure 2: CP-averaged angular coefficients $S_i^{(a)}$, CP-averaged dilepton mass distribution $d(\Gamma + \bar{\Gamma})/dq^2$ and transverse asymmetries $A_T^{(3,4)}$ in the SM as a function of q^2 . The dashed lines are the leading-order (LO) contributions, obtained in naïve factorization. The thick solid lines are the full next-to-leading order (NLO) predictions from QCD factorization (QCDF), as described in Sec. 2.4. The blue band defines the total error for the NLO result as described in the text.

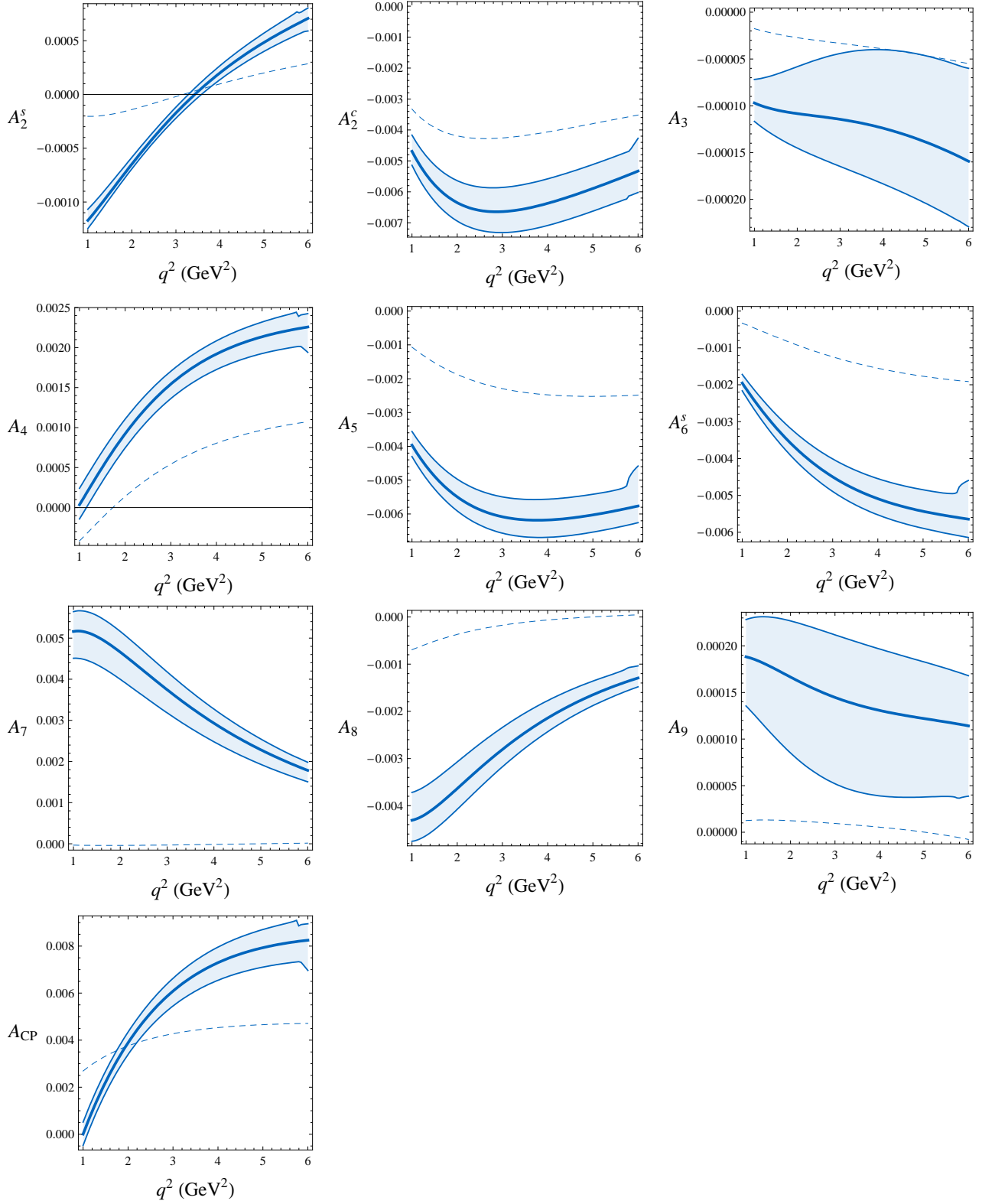


Figure 3: CP asymmetries $A_i^{(a)}$ and A_{CP} in the SM as a function of q^2 . The meaning of the curves and bands is as in Fig. 2.

Obs.	$10^3 \times \dots$	Obs.	$10^3 \times \dots$
$\langle A_1^s \rangle$	$-1.2^{+1.1}_{-1.0}$	$\langle A_5 \rangle$	$-28.9^{+3.0}_{-2.3}$
$\langle A_1^c \rangle$	$31.5^{+3.4}_{-3.9}$	$\langle A_6^s \rangle$	$-22.5^{+2.5}_{-2.0}$
$\langle A_2^s \rangle$	$-0.3^{+0.4}_{-0.4}$	$\langle A_7 \rangle$	$17.2^{+1.9}_{-2.5}$
$\langle A_2^c \rangle$	$-30.5^{+3.8}_{-3.3}$	$\langle A_8 \rangle$	$-13.0^{+2.1}_{-1.6}$
$\langle A_3 \rangle$	$-0.5^{+0.4}_{-0.3}$	$\langle A_9 \rangle$	$0.5^{+0.3}_{-0.4}$
$\langle A_4 \rangle$	$7.7^{+0.9}_{-1.0}$	$\langle A_{\text{CP}} \rangle$	$29.7^{+3.1}_{-3.4}$

Table 7: Predictions for the integrated CP asymmetries $\langle A_i^{(a)} \rangle$ (in units of 10^{-3}) in the SM. Note the different normalization with respect to Ref. [20], see footnote 6.

As explained in Sec. 5, the CP asymmetries are close to zero in the SM, which is evident from Fig. 3, where we show all the $A_i^{(a)}$ (again except for $A_1^{s,c}$) and the CP asymmetry in the decay distribution, A_{CP} . As explained above, the shift from LO to NLO is substantial. Our results are in good agreement with Ref. [20], but do not coincide exactly. This can be understood by recalling that we use the full LCSR form factors and that our normalization of the soft form factors, especially ξ_{\parallel} , is different from that used in Ref. [20]. Also our choice of quark masses, in particular m_c/m_b and m_t , as well as the scale μ at which the QCDF hard-scattering corrections are evaluated, differs from [20]. We stress that, in view of the smallness of the SM values of A_i , these discrepancies become irrelevant once large NP contributions start to dominate these observables, as we shall see in the remainder of this section.

In Tab. 7, we list our predictions for the q^2 -integrated CP asymmetries as defined in Eq. (5.12).

6.2 Model-independent Considerations

Before turning to specific NP scenarios, we investigate the model-independent impact of the Wilson coefficients on our observables.

6.2.1 Impact of Wilson Coefficients on Observables

The impact of NP on the angular observables discussed in our paper is given by the changes of the Wilson coefficients of the affected operators. One can group these Wilson coefficients into three classes:

- Dipole coefficients: C_7 , C'_7 , C_8 and C'_8 . The role of the gluon dipole operators is sub-leading in the decay considered.
- Semileptonic coefficients: C_9 , C'_9 , C_{10} and C'_{10} .
- Scalar coefficients: $C_S - C'_S$ and $C_P - C'_P$.

Before entering the discussion of various NP scenarios, it is useful to study the correlation between the angular coefficients and the Wilson coefficients. In Tab. 8 we show which observables are most affected by a significant change of a given coefficient. In Tab. 9 we show,

Wilson coefficients	largest effect in
C_7, C'_7	$S_1^s, S_1^c, S_2^s, S_2^c, S_3, S_4, S_5, S_6^s,$ $A_7, A_8, A_9,$ $\text{BR}(B \rightarrow X_s \gamma), \text{BR}(B \rightarrow X_s \mu^+ \mu^-)$
$C_9, C'_9, C_{10}, C'_{10}$	$S_1^s, S_1^c, S_2^s, S_2^c, S_3, S_4, S_5, S_6^s,$ $A_7, A_8, A_9,$ $\text{BR}(B \rightarrow X_s \mu^+ \mu^-)$
$C_S - C'_S$	$S_6^c,$ $\text{BR}(B_s \rightarrow \mu^+ \mu^-)$
$C_P - C'_P$	$S_1^c + S_2^c,$ $\text{BR}(B_s \rightarrow \mu^+ \mu^-)$

Table 8: The Wilson coefficients relevant in $B \rightarrow K^* \mu^+ \mu^-$ and the observables they have the largest impact on.

on the other hand, which Wilson coefficients should be altered to produce a large effect in specific observables.

We observe:

- $C_7, C'_7, C_9, C'_9, C_{10}$ and C'_{10} can induce large effects in many observables, or at least in those that do not require the presence of strong phases. To be precise, the A_i are mainly induced by imaginary parts of the Wilson coefficients, while the S_i are induced by their real parts.
- Only the primed coefficients C'_7, C'_9 and C'_{10} can significantly affect the observables S_3 and A_9 . As can be seen from Eq. (5.10), S_3 corresponds to the transverse asymmetry $A_T^{(2)}$ and the impact of NP physics contributions to C'_7 on this observable has been studied for example in Refs. [21, 44, 46].
- The scalar operators affect mainly S_6^c and the branching ratio for $B_s \rightarrow \mu^+ \mu^-$. This implies interesting correlations between these two observables as discussed in Sec. 6.2.3.

6.2.2 Model-independent Analysis of S_4, S_5 and S_6^s

The zero of the forward-backward asymmetry has been the focus of many experimental and theoretical studies (see for example Refs. [10, 17]) as it is established as being an observable free from hadronic effects and capable of distinguishing between NP scenarios. In Sec. 5 we expressed the CP-averaged forward-backward asymmetry in terms of S_6^s through Eq. (5.7), so S_6^s could clearly be studied instead of A_{FB} . In addition, from Fig. 2, we find there are two more observables with such a zero in q^2 , S_4 and S_5 . A study of these three observables in a model-independent way could allow us to constrain the NP contributions to the Wilson coefficients.

From Tab. 9 we see that the zero of $S_4, q_0^2(S_4)$, is largely sensitive to C_7, C'_7, C_{10} and C'_{10} . This dependence arises only through $C_7 - C'_7$ and $C_{10} - C'_{10}$. We therefore explore how the position of the zero in q^2 is affected by NP modifications to $C_{10} - C'_{10}$ and C_7 . The current

Observable	mostly affected by
$S_1^s, S_1^c, S_2^s, S_2^c$	$C_7, C_7', C_9, C_9', C_{10}, C_{10}'$
S_3	C_7', C_9', C_{10}'
S_4	$C_7, C_7', C_{10}, C_{10}'$
S_5	C_7, C_7', C_9, C_{10}'
S_6^s	C_7, C_9
A_7	$C_7, C_7', C_{10}, C_{10}'$
A_8	$C_7, C_7', C_9, C_9', C_{10}'$
A_9	C_7', C_9', C_{10}'
S_6^c	$C_S - C_S'$

Table 9: The most interesting angular observables in $B \rightarrow K^* \mu^+ \mu^-$ and the Wilson coefficients they are most sensitive to.

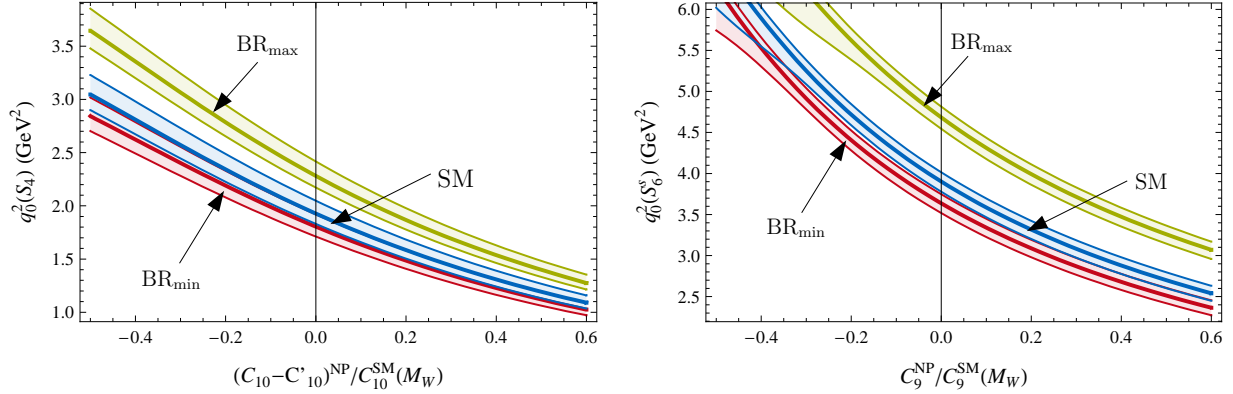


Figure 4: Left: correlation between $q_0^2(S_4)$, the position of the zero of S_4 , and the NP contribution to $C_{10} - C_{10}'$. Right: correlation between $q_0^2(S_6^c)$ and C_9 . We use the branching ratio for $B \rightarrow X_s \gamma$ to constrain the NP contributions to C_7 and C_7' . The green (red) band corresponds to a value of $\text{BR}(B \rightarrow X_s \gamma)$ at the upper (lower) end of the experimental 2σ range, the blue band to SM values for C_7, C_7' .

experimental value of the branching ratio of $B \rightarrow X_s \gamma$ provides a constraint on C_7 and C_7' . We find a strong dependence of $q_0^2(S_4)$ on $C_{10} - C_{10}'$, and its measurement would provide very interesting information about these Wilson coefficients. In Fig. 4, we show this dependence for real values of C_7 .

If the NP introduces an imaginary phase to C_7 , the bound from $B \rightarrow X_s \gamma$ is weakened, allowing large effects in the zeros. In fact, the large values of $\text{Im}(C_7)$ significantly enhance the branching ratio of the decay $B \rightarrow X_s \gamma$ and in order to be in agreement with the experimental data, large positive contributions to $\text{Re}(C_7)$ that interfere destructively with C_7^{SM} are required⁸. Exactly these large positive contributions to $\text{Re}(C_7)$ then unambiguously shift the zeros of S_4, S_5 and S_6^s towards lower values.

⁸We note that, for such values of the Wilson coefficients, the branching ratio of the decay $B \rightarrow X_s \mu^+ \mu^-$ is largely enhanced to values of around $\text{BR}(B \rightarrow X_s \mu^+ \mu^-) \simeq 2.5 \times 10^{-6}$, close to the experimental 2σ upper bound.

This analysis can also be applied to S_6^s , which depends strongly on C_7 and C_9 . We examine the dependence of $q_0^2(S_6^s)$ on NP contributions to C_9 and C_7 . This again is restricted by the experimental value of the branching ratio of $B \rightarrow X_s \gamma$. We find a strong dependence on C_9 , and for real values of C_7 this would be a clean way to determine information about a possible NP contribution to C_9 as seen in Fig 4. Again, if NP induces a complex phase of C_7 , the range in $q_0^2(S_6^s)$ increases dramatically.

It is a greater challenge to extract information about the Wilson coefficients from S_5 due to its dependence on C_7 , C_7' , C_9 and C_{10}' . However, a measurement of $q_0^2(S_5)$ could provide a consistency check with $C_{10} - C_{10}'$ and C_9 determined from S_4 and S_6 , provided C_7 , C_7' are real. In addition, this might allow one to untangle the effects of C_{10}^{NP} and $C_{10}'^{\text{NP}}$ in Fig. 4.

6.2.3 Impact of Scalar Currents

As mentioned in the introduction, the impact of the scalar and pseudoscalar operators $\mathcal{O}_{S,P}^{(\prime)}$ on the angular distribution of $B \rightarrow K^*(\rightarrow K\pi)\mu^+\mu^-$ has been considered before [43], and no relevant effects on the observables of interest were found. However, as shown in Sec. 3.2, the inclusion of lepton-mass effects⁹, which were neglected in previous studies, gives rise to an additional observable in models with scalar currents, which can serve as a precision null-test of the SM and, as we will show, in principle allows one to distinguish between different NP models.

To assess the size of the possible effects generated by these operators, we first consider the allowed ranges for the Wilson coefficients $C_{S,P}^{(\prime)}$. The most stringent constraint on these coefficients comes from the measurement of $B_s \rightarrow \mu^+\mu^-$, which is strongly helicity suppressed in the SM, with a predicted branching ratio of [50, 51]

$$\text{BR}(B_s \rightarrow \mu^+\mu^-) = (3.37 \pm 0.31) \times 10^{-9}. \quad (6.1)$$

The most recent experimental upper bound still lies, at the 95% confidence level, one order of magnitude above the SM [76]:

$$\text{BR}(B_s \rightarrow \mu^+\mu^-) < 5.8 \times 10^{-8}. \quad (6.2)$$

However, in many models, e.g. the MSSM at large $\tan\beta$, this branching ratio can be greatly enhanced.

In a generic NP model, the branching ratio is given by

$$\text{BR}(B_s \rightarrow \mu^+\mu^-) = \tau_{B_s} f_{B_s}^2 m_{B_s} \frac{\alpha_{\text{em}}^2 G_F^2}{16\pi^3} |V_{tb} V_{ts}^*|^2 \sqrt{1 - \frac{4m_\mu^2}{m_{B_s}^2}} \left[|S|^2 \left(1 - \frac{4m_\mu^2}{m_{B_s}^2} \right) + |P|^2 \right], \quad (6.3)$$

where

$$S = \frac{m_{B_s}^2}{2} (C_S - C_S'), \quad P = \frac{m_{B_s}^2}{2} (C_P - C_P') + m_\mu (C_{10} - C_{10}'). \quad (6.4)$$

Considering the experimental bound in Eq. (6.2), these formulae imply the approximate bounds

$$|C_S - C_S'| \lesssim 0.12 \text{ GeV}^{-1}, \quad -0.09 \text{ GeV}^{-1} \lesssim C_P - C_P' \lesssim 0.15 \text{ GeV}^{-1}, \quad (6.5)$$

barring large NP contributions to the Wilson coefficients $C_{10}^{(\prime)}$.

⁹We stress that we restricted ourselves to muons in our numerical analysis.

Now, inspecting the formulae for the angular coefficients, Eqs. (3.34)–(3.45), one can see that the only terms in which $C_S^{(\prime)}$ and $C_P^{(\prime)}$ are not suppressed by the lepton mass enter in the angular coefficient I_1^c . However, due to the small size of the Wilson coefficients themselves, see (6.5), these terms turn out to be numerically irrelevant in general once the bound from $B_s \rightarrow \mu^+ \mu^-$ is taken into account.

Since the pseudoscalar operators do not contribute to any other angular coefficient, this implies that they are indeed irrelevant in the phenomenological study of $B \rightarrow K^*(\rightarrow K\pi)\mu^+\mu^-$. For the scalar operators, however, the situation is different, because of the new angular coefficient I_6^c , Eq. (3.41), which is directly proportional to the real part of $(C_S - C'_S)$ and thus vanishes in the SM. So, although numerically small, this angular coefficient is an appealing observable because any measurement of a non-zero value would constitute an unambiguous signal of scalar currents at work.

This is in contrast to the process $B_s \rightarrow \mu^+ \mu^-$, where a large enhancement of the branching ratio compared to the SM could be caused by both scalar and pseudoscalar currents. In addition, the measurement of a non-zero S_6^c (the CP-averaged counterpart of I_6^c) would allow to determine the sign of $\text{Re}(C_S - C'_S)$. In fact, by a combined study of $B_s \rightarrow \mu^+ \mu^-$ and the observable S_6^c , one would be able to constrain the relative sizes of the scalar and pseudoscalar Wilson coefficients, which can serve to distinguish different models of NP. For example, in the MSSM, the ratio of C_S and C_P is

$$\frac{C_P}{C_S} \approx -\frac{M_{A_0}^2}{M_{H^0}^2} \approx -1 \quad (6.6)$$

to a very good accuracy, a relation which could be tested by a measurement of $\text{BR}(B_s \rightarrow \mu^+ \mu^-)$ and S_6^c .

To illustrate this point, we show, in Fig. 5, the correlation between $\text{BR}(B_s \rightarrow \mu^+ \mu^-)$ and $\langle S_6^c \rangle$ (as defined in Eq. (5.11)). The blue band has been obtained by assuming that NP contributions enter only through C_S , i.e. setting $C_P/C_S = 0$, and varying C_S accordingly; the error band takes into account all the sources of error as discussed in Sec. 6.1.

Assuming, in contrast, $C_P/C_S = -1$, as would be the case in the MSSM, one obtains the black dashed parabola. As an illustration, the predictions for parameter points in the constrained MSSM (CMSSM) with large $\tan\beta$ are indicated as red and green dots. These points have been generated by a random scan of the CMSSM parameters in the ranges

$$m_0 \leq 1 \text{ TeV}, \quad m_{1/2} \leq 1 \text{ TeV}, \quad (6.7)$$

$$-2m_0 \leq A_0 \leq 2m_0, \quad 30 \leq \tan\beta \leq 50, \quad (6.8)$$

permitting both signs for the μ -term and discarding points violating existing mass bounds or being incompatible with the measurement of $\text{BR}(B \rightarrow X_s \gamma)$. The green dots correspond to $\mu > 0$, the red ones to $\mu < 0$. It can be seen that the CMSSM points lie on the curve corresponding to $C_S = -C_P$ and, in particular for a positive μ parameter, could be clearly distinguished from the scenario without pseudoscalar currents, assuming sufficient experimental accuracy.

Since the observable $\langle S_6^c \rangle$ probes the real part of $(C_S - C'_S)$, the correlation gets modified if one allows a phase in C_S . More precisely, $|\langle S_6^c \rangle|$ gets reduced for a fixed value of $\text{BR}(B_s \rightarrow \mu^+ \mu^-)$. This is illustrated by the black curves corresponding to $C_S = -C_P$, where both Wilson coefficients are now complex, with the respective phase $\text{Arg}(C_S)$ indicated by the labels on

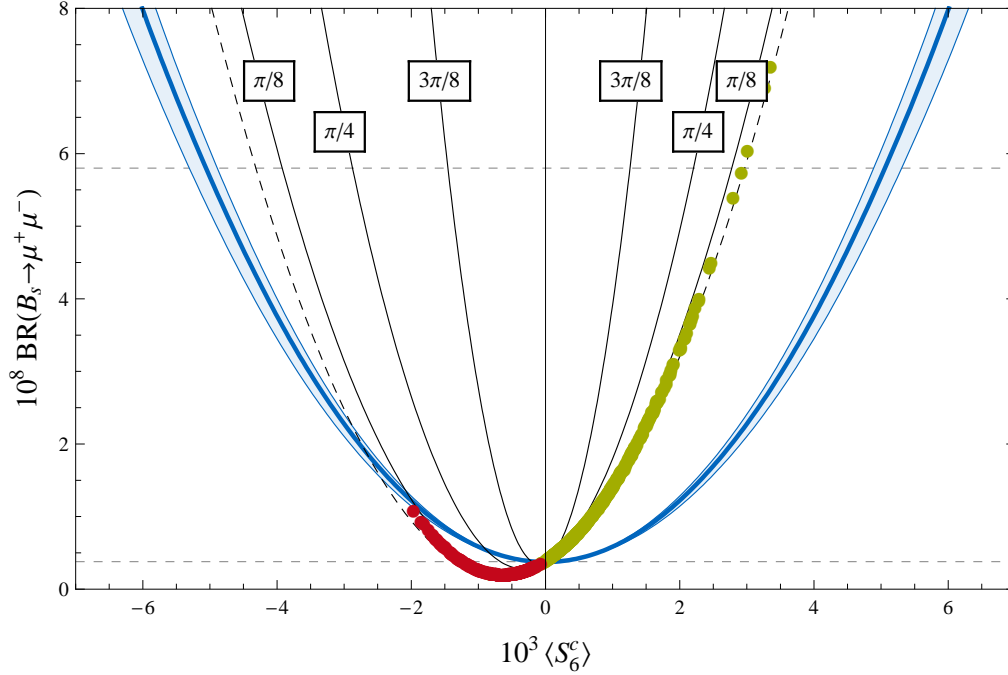


Figure 5: Correlation between the observable $\langle S_6^c \rangle$ and the branching ratio of $B_s \rightarrow \mu^+ \mu^-$. The blue band is obtained by assuming NP contributions only to the Wilson coefficient C_S , the black curves (where error bars are omitted) by assuming $C_P = -C_S$. Different values of the phase $\text{Arg}(C_S)$ are indicated. The red and green dots correspond to points in the CMSSM as described in the text. The horizontal dashed lines indicate the SM prediction for $\text{BR}(B_s \rightarrow \mu^+ \mu^-)$ (6.1) and the current experimental upper bound (6.2).

the curves. This is precisely what happens in the Flavour Blind MSSM discussed in detail in Sec. 6.3.2. In this scenario, the measurement of the correlation between $\text{BR}(B_s \rightarrow \mu^+ \mu^-)$ and $\langle S_6^c \rangle$ would thus directly probe the phase of the scalar Wilson coefficient.

To summarize, while pseudoscalar operators are numerically irrelevant in the decay $B \rightarrow K^*(\rightarrow K\pi)\mu^+\mu^-$, a study of the angular distribution allows one to probe the scalar sector of a theory beyond the SM, in a way that is theoretically clean and complementary to $B_s \rightarrow \mu^+\mu^-$.

6.3 Specific New Physics Scenarios

With the SM predictions for the CP-averaged angular coefficients $S_i^{(a)}$ and the CP asymmetries $A_i^{(a)}$ in hand, we now investigate how these observables change in the NP scenarios discussed in Sec. 4.

6.3.1 Minimal Flavour Violation

In the MFV framework as described in Sec. 4.3, no additional CP-violating phases are present and NP contributions to the Wilson coefficients of the primed operators can be neglected. This implies that all possible effects will arise from real contributions to the Wilson coefficients C_7 , C_8 , C_9 and C_{10} . This implies in turn that the most visible departures from the SM predictions will be in the observables $S_{1,2}^{s,c}$, S_4 , S_5 and S_6^s , while the other angular observables

and in particular the CP asymmetries will essentially be SM like.¹⁰

Model-independent studies within the MFV framework show that large NP contributions to the Wilson coefficients C_7 , C_8 , C_9 and C_{10} are still allowed [77]. In particular, scenarios in which the sign of these Wilson coefficients is flipped with respect to the SM cannot yet be excluded.

However, in concrete MFV NP models it is usually difficult to generate large effects in C_9 and C_{10} . For example in the MFV MSSM, NP contributions to C_9 and C_{10} are typically very small [72, 78]. Therefore, in this model, the main source of NP effects is C_7 whose value can be modified substantially by chargino-stop loops. For negligible NP contributions to C_9 and C_{10} however, the effects in C_7 are strongly constrained by the data on $\text{BR}(B \rightarrow X_s \gamma)$ and $\text{BR}(B \rightarrow X_s \mu^+ \mu^-)$ and in particular a sign flip in C_7 is excluded at the 3σ level [79]. The effects in the $S_i^{(a)}$ are then quite limited. In Fig. 6, we show the largest possible effects in S_4 , S_5 and S_6^s : scenario MFV_I (green curves) corresponds to the maximum allowed negative (i.e. constructive) NP contribution to C_7 (i.e. C_7^{NP}) and shifts the zeros of S_4 , S_5 and S_6^s to larger values of q^2 . Scenario MFV_{II} (red curves), on the other hand, corresponds to the largest positive allowed value of C_7^{NP} and hence shifts the zeros to smaller values. The separation in q^2 between these two curves corresponds to the range shown in Fig. 4 for $(C_{10}^{\text{NP}} - C_{10}'^{\text{NP}}) = 0$ and $C_9^{\text{NP}} = 0$, respectively, where the superscript NP denotes the NP contribution to the Wilson coefficient. The most relevant input parameters corresponding to the two scenarios are collected in Tab. 10.

Scenario	$\tan \beta$	m_A	$m_{\tilde{g}}$	$m_{\tilde{Q}}$	$m_{\tilde{U}}$	$A_{\tilde{t}}$	μ
MFV _I	28	380	530	800	540	-850	860
MFV _{II}	29	530	1000	880	660	880	750

Table 10: Most relevant parameters of the two MFV MSSM scenarios discussed in the text. $\tan \beta$ is the ratio of the two Higgs VEVs, m_A the mass of the pseudoscalar Higgs, $m_{\tilde{g}}$ is the gluino mass, $m_{\tilde{Q}}$ is a universal soft mass for the left handed squark doublets, $m_{\tilde{U}}$ a universal soft mass for the right handed up squarks, $A_{\tilde{t}}$ is the stop trilinear coupling and μ the Higgsino mass parameter. Our conventions for the trilinear coupling are such that the left-right mixing entry in the stop mass matrix is $(m^2)_{LR} = -m_t(A_{\tilde{t}} + \mu^* \cot \beta)$. All massive parameters are given in GeV.

It is well known that in the MFV MSSM, the shift in the zero of the forward-backward asymmetry in $B \rightarrow X_s \mu^+ \mu^-$ is highly correlated with a change of the branching ratio of $B \rightarrow X_s \gamma$ [80, 81]. In Fig. 7 we show the corresponding correlation between the zeros of S_4 , S_5 and S_6^s and $\text{BR}(B \rightarrow X_s \gamma)$. Any deviation from the lines in the plots would signal the presence either of NP contributions to Wilson coefficients other than C_7 or of new CP-violating phases that lead to complex values of C_7 .

6.3.2 Flavour Blind MSSM

One model with new sources of CP violation is the FBMSSM discussed in Refs. [55, 56, 57, 58]. This is a MSSM where the CKM matrix is the only source of flavour violation, but additional CP-violating, flavour conserving phases are present in the soft sector. Within this framework,

¹⁰ In general the concept of MFV does not exclude effects in the scalar Wilson coefficient C_S which affect the observable S_6^c . However, as shown in Sec. 6.2.3, these effects can be discussed completely independently and we will not consider them in this section.

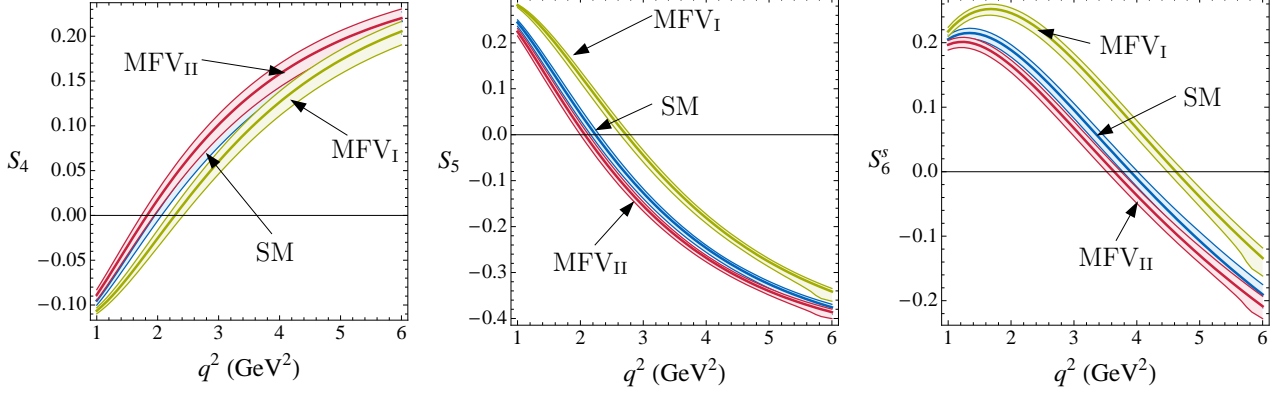


Figure 6: The observables S_4 , S_5 and S_6^s in the SM (blue band) and the MFV MSSM scenarios MFV_{I,II} described in the text.

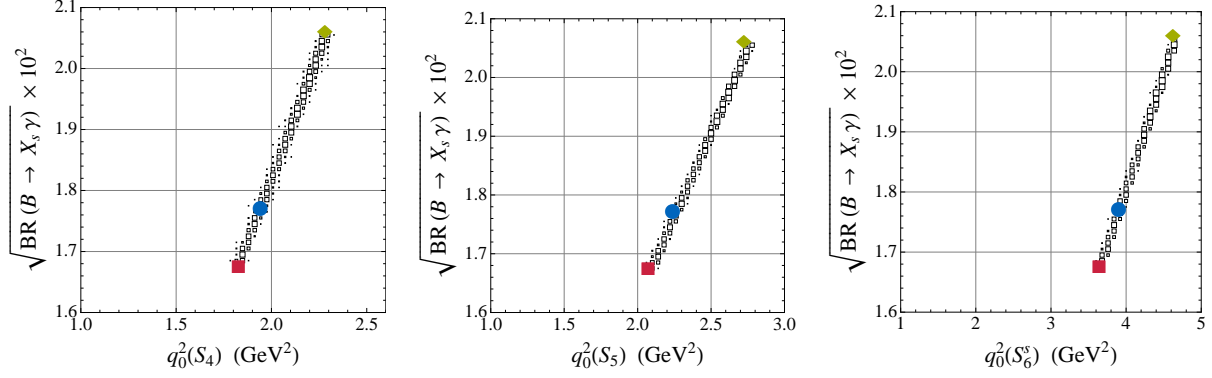


Figure 7: The correlation between the zeros of S_4 , S_5 and S_6^s and $\text{BR}(B \rightarrow X_s \gamma)$ in the MFV MSSM. The blue circles correspond to the central SM values, while the green diamonds represent scenario MFV_I and the red squares scenario MFV_{II}.

the majority of non-standard effects arises though complex NP contributions to the Wilson coefficient C_7 . We discuss two scenarios in which the effects are maximal: scenario FBMSSM_I is characterized by large negative $\text{Im}(C_7)$, while scenario FBMSSM_{II} corresponds to a large positive $\text{Im}(C_7)$. The corresponding input parameters are collected in Tab. 11, together with those of a third scenario, FBMSSM_{III}, to be considered later.

Concerning the CP asymmetries, we observe that significant departures from the SM predictions can be obtained in $A_{1,2}^s$, A_5 , A_6^s , A_7 and A_8 . The most pronounced effects can be seen in A_7 and A_8 and these are shown in the left and centre plot of Fig. 8. The effects here are predominantly due to the large imaginary part of C_7 and we note that in this case

Scenario	$\tan \beta$	m_A	$m_{\tilde{g}}$	$m_{\tilde{Q}}$	$m_{\tilde{U}}$	$A_{\tilde{t}}$	μ	$\text{Arg}(\mu A_{\tilde{t}})$
FBMSSM _I	40	400	700	380	700	900	150	-45°
FBMSSM _{II}	40	400	700	380	700	900	150	50°
FBMSSM _{III}	40	400	700	550	700	900	150	-60°

Table 11: Most relevant parameters of the three FBMSSM scenarios discussed in the text. All massive parameters are given in GeV.

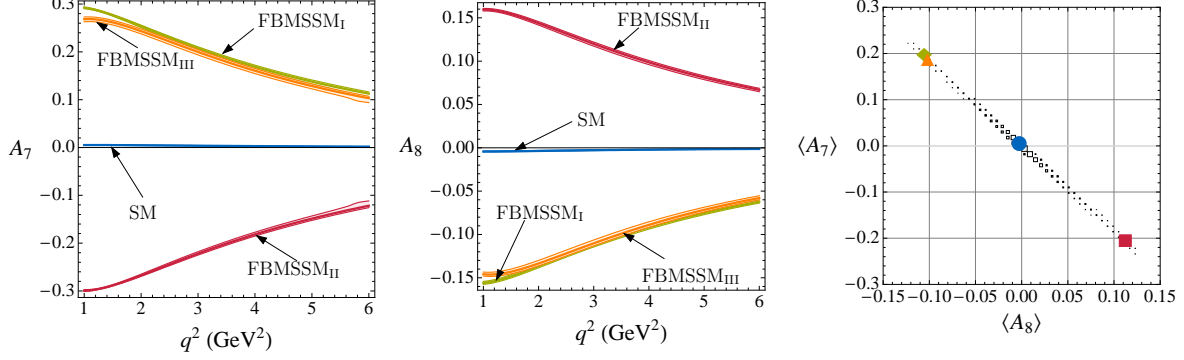


Figure 8: Left and centre plot: CP asymmetries A_7 and A_8 in the SM (blue band) and three FBMSSM scenarios as described in the text. Right plot: correlation between the integrated asymmetries $\langle A_7 \rangle$ and $\langle A_8 \rangle$ in the FBMSSM. Blue circle: SM, green diamond: FBMSSM_I, red square: FBMSSM_{II}, orange triangle: FBMSSM_{III}.

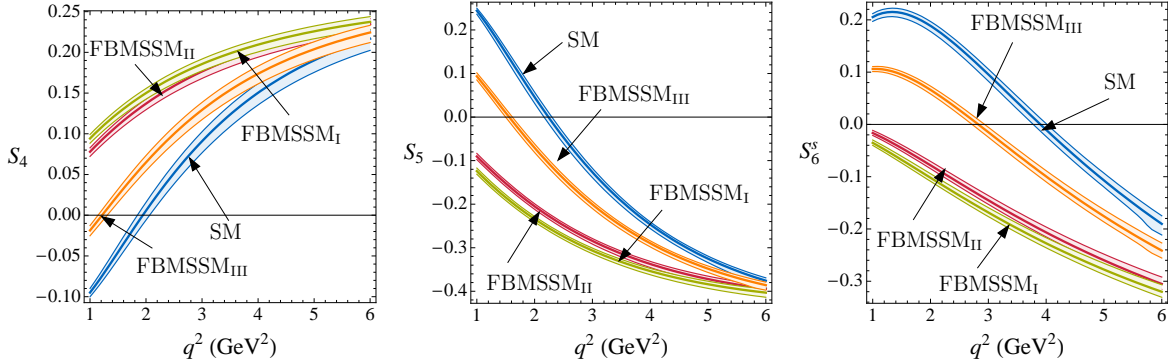


Figure 9: The observables S_4 , S_5 and S_6^s in the SM (blue band) and the three FBMSSM scenarios FBMSSM_{I,II,III}.

positive values for A_7 imply negative ones for A_8 and vice versa. This is also displayed in the right plot of Fig. 8, where we show the almost perfect correlation between the integrated asymmetries $\langle A_7 \rangle$ and $\langle A_8 \rangle$. Any deviation from the line shown in this plot would signal the presence of additional imaginary parts in either $C_7^{(r)}$ or $C_9^{(r)}$ and $C_{10}^{(r)}$.

In the CP-averaged angular coefficients we find significant departures from the SM in $S_{1,2}^{s,c}$, S_4 , S_5 , S_6^s and also in S_6^c , while effects in S_3 , S_7 , S_8 and S_9 can hardly be distinguished from the SM. Although in the FBMSSM the $\text{BR}(B_s \rightarrow \mu^+ \mu^-)$ can be close to its experimental upper bound, the effects in S_6^c are smaller than the maximal effects found in the model independent-discussion of Sec. 6.2.3, because the large imaginary part in C_7 implies a large phase for the relevant Wilson coefficient C_S . Concerning $S_{1,2}^{s,c}$, we find that while $|S_{1,2}^s|$ is enhanced, $|S_{1,2}^c|$ is suppressed with respect to the SM results. For S_4 , S_5 and the forward-backward asymmetry S_6^s we find significant shifts in their zero towards values of q^2 lower than the SM prediction or we even find no zero at all. These effects are shown in Fig. 9 and are much larger than those possible in the MFV MSSM (see Fig. 6). The reason for these large shifts are the large values of $\text{Im}(C_7)$ in the scenarios considered, as discussed in Sec. 6.2.2.

One finds that the strict correlation between the zeros and $\text{BR}(B \rightarrow X_s \gamma)$ is lost in the FBMSSM. This is shown in the upper plots of Fig. 10. However, as the additional contributions to $b \rightarrow s \gamma$ from the imaginary part of C_7 can only enhance the branching ratio,

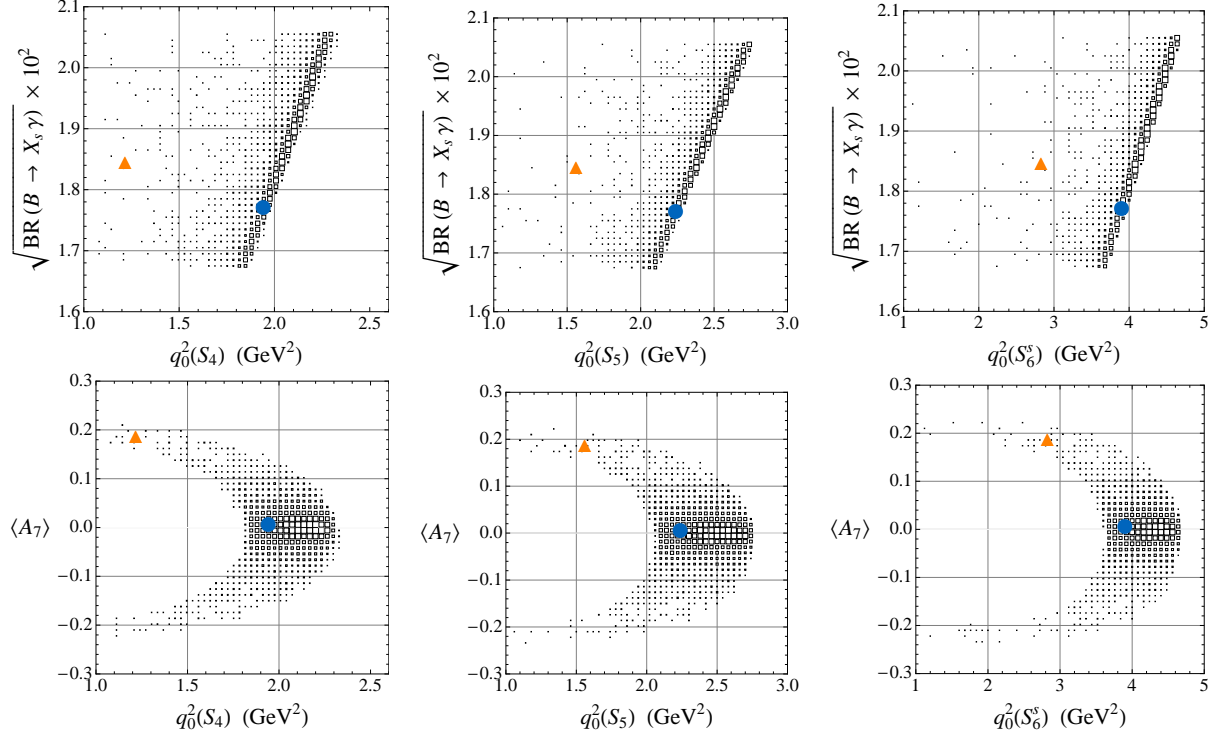


Figure 10: Correlation between the zeros of S_4 , S_5 and S_6^s with the $b \rightarrow s\gamma$ branching ratio (upper plots) and with the integrated asymmetry $\langle A_7 \rangle$ (lower plots) in the FBMSM. The blue circles correspond to the SM predictions. The orange triangles correspond to a FBMSM scenario that gives $S_{\phi K_S}$ close to the central experimental value $\simeq 0.44$.

one still finds an upper bound on the zeros for a given value of $\text{BR}(B \rightarrow X_s \gamma)$. In addition, in the lower plots of Fig. 10 we show the zeros $q_0^2(S_4)$, $q_0^2(S_5)$ and $q_0^2(S_6^s)$ against the integrated asymmetry $\langle A_7 \rangle$. One observes that large effects in $\langle A_7 \rangle$ are correlated with large shifts in the zeros towards lower values.

In order to identify signs in the CP asymmetries which are favoured in this model one must include additional observables in the analysis. To this end we also investigate the direct CP asymmetry in the $b \rightarrow s\gamma$ decay $A_{\text{CP}}(b \rightarrow s\gamma)$, the electric dipole moments of the electron and the neutron d_e and d_n and the mixing induced CP asymmetry $S_{\phi K_S}$. We recall that in [58] striking correlations between these observables have been found. In particular, the desire to explain the anomaly observed in $S_{\phi K_S}$ through the presence of flavour conserving but CP-violating phases implied a positive $A_{\text{CP}}(b \rightarrow s\gamma)$, by an order of magnitude larger than its SM tiny value and d_e , d_n at least as large as 10^{-28} e cm .

The left plot of Fig. 11 shows the correlation between $\langle A_7 \rangle$ and $S_{\phi K_S}$. We find that a value of $S_{\phi K_S} \simeq 0.44$, as indicated by the present data [82], implies a positive value for $\langle A_7 \rangle$ in the range $[0.05, 0.2]$ and then also a negative value for $\langle A_8 \rangle$ in the range $[-0.11, -0.03]$. In addition to the two scenarios discussed above, we have chosen also a third scenario, FBMSM_{III}, indicated as orange triangle in the plots of Figs. 8, 10 and 11, that gives $S_{\phi K_S}$ close to the experimental value. This scenario is shown in Figs. 8 and 9 as the orange bands and we find that while one still can get almost maximal effects in $\langle A_7 \rangle$ and $\langle A_8 \rangle$ the effects in S_4 , S_5 and S_6^s are much less pronounced.

In the centre plot of Fig. 11 we report the correlation between $\langle A_7 \rangle$ and $A_{\text{CP}}(b \rightarrow s\gamma)$. One observes that positive values for $\langle A_7 \rangle$ imply positive values for $A_{\text{CP}}(b \rightarrow s\gamma)$ that can

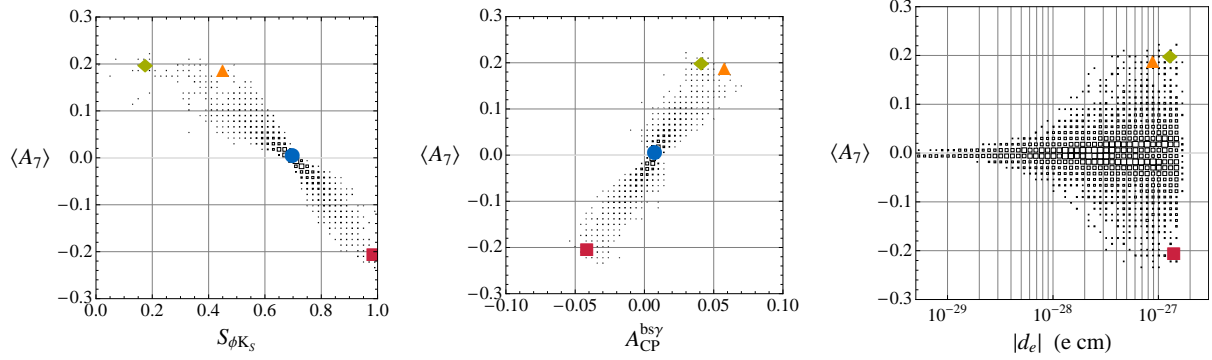


Figure 11: $\langle A_7 \rangle$ vs. $S_{\phi K_S}$ (left plot), $\langle A_7 \rangle$ vs. $A_{CP}^{bs\gamma}$ (centre plot) and $\langle A_7 \rangle$ vs. d_e (right plot) in the FBMSSM. The blue circles correspond to the SM, while the red square (green diamond) corresponds to scenario 1 (2) discussed in the text. Finally the orange triangle indicates a parameter point that also gives $S_{\phi K_S}$ close to its experimental value of $\simeq 0.44$.

Scenario	f	x_L	m_H^1	m_H^2	m_H^3	θ_{23}^d	θ_{13}^d	θ_{12}^d	δ_{23}^d	δ_{13}^d	δ_{12}^d
LHT _I	1000	0.5	565	1000	770	1.60	2.50	1.35	5.70	4.20	5.80
LHT _{II}	1000	0.5	1000	375	425	1.50	1.00	4.75	4.25	0.60	2.85

Table 12: Parameters of the LHT scenarios LHT_{I,II}: θ_{ij}^d and δ_{ij}^d are the parameters of the CKM-like unitary mixing matrix for the mirror d quarks, m_H^i are the masses of the mirror quarks, f is the high energy scale and x_L the mixing parameter of the SM top and the T-even top partner.

reach values up to $(6 - 7)\%$.

Finally, the right plot of Fig. 11 shows the correlation between $\langle A_7 \rangle$ and the EDM of the electron, d_e in the FBMSSM. We find that large values for $\langle A_7 \rangle$ necessarily require large values for the electron EDM close to the current upper bound of $1.6 \times 10^{-27} e \text{ cm}$ [83].

6.3.3 LHT

We analyse the angular observables within the LHT by means of a global parameter scan taking into account all relevant constraints from other flavour observables. As already anticipated in Ref. [64], most NP effects in the observables considered here are found to be small. In particular S_6^s , the forward-backward asymmetry, turns out to be very close to the SM. The same applies to all other CP-averaged angular coefficients and most CP asymmetries. The largest effects relative to the SM are found in A_7 and A_8 as in the SM their absolute values are at most 6×10^{-3} and 5×10^{-3} , respectively. We consider two scenarios, LHT_I and LHT_{II}, with input parameters as given in Tab. 12. In the left and centre plot of Fig. 12 we show the corresponding asymmetries A_7 and A_8 as functions of q^2 . The blue curves represent the SM. The green curves labelled LHT_I correspond to a LHT parameter point that gives the largest negative NP contribution to $\text{Im}(C_9)$ and $\text{Im}(C_{10})$, while the LHT_{II} curves (red) give the largest positive contribution. Enhancement of both asymmetries by a factor of three is possible for low values of q^2 with visible but smaller effects for larger values of q^2 .

Still, these significant enhancements are one order of magnitude smaller than those found in the FBMSSM. The reason why much larger effects in A_7 and A_8 are possible in the latter model is that large NP contributions to the imaginary part of C_7 are allowed, comparable in

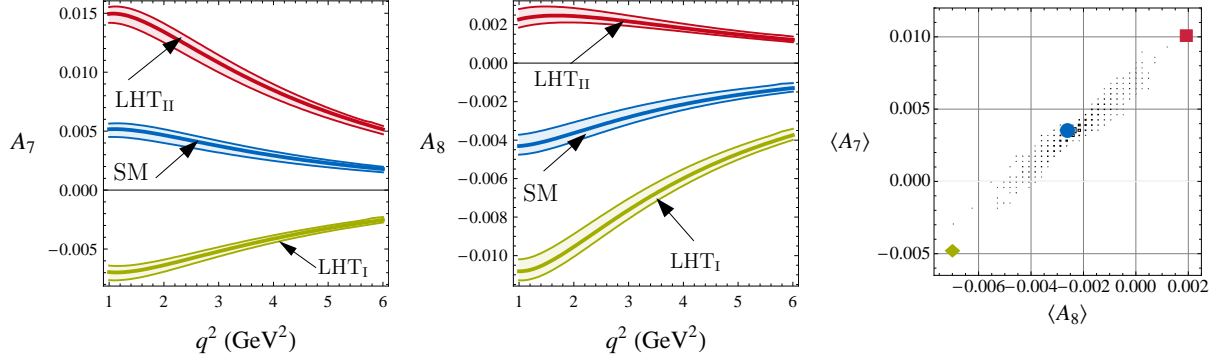


Figure 12: Left and centre plot: CP asymmetries A_7 and A_8 in the SM (blue band) and the LHT scenarios $LHT_{I,II}$. Right plot: Correlation between the integrated asymmetries $\langle A_7 \rangle$ and $\langle A_8 \rangle$ in the LHT. The blue circle represents the SM, the green diamond scenario LHT_I and the red square scenario LHT_{II} .

Scenario	$\tan \beta$	m_A	$m_{\tilde{g}}$	$m_{\tilde{Q}}$	$m_{\tilde{U}}$	$m_{\tilde{D}}$	$A_{\tilde{u}}$	$A_{\tilde{d}}$	μ	$ (\delta_d)_{32}^{LR} $	$\text{Arg}(\delta_d)_{32}^{LR}$
GMSSM _I	6	520	500	400	500	380	800	750	470	0.01	-135°
GMSSM _{II}	5	740	1000	460	1000	390	1500	440	200	0.03	60°

Table 13: Most relevant parameters of the two general MSSM scenarios with large C'_7 as discussed in the text. $m_{\tilde{D}}$ a universal soft mass for the right handed down squarks, $A_{\tilde{u}(\tilde{d})}$ universal trilinear couplings for the up (down) squarks and $(\delta_d)_{32}^{LR}$ the left-right mass insertion that generates large effects in C'_7 . Our conventions for the trilinear coupling are such that the left-right mixing entry in the sbottom mass matrix is $(m^2)_{LR} = -m_b(A_{\tilde{d}} + \mu^* \tan \beta)$. All massive parameters are given in GeV.

magnitude to the SM contribution. In the LHT model NP contributions to C_7 are found to be very small [64]. As the effects in A_7 and A_8 are therefore dominantly created by $\text{Im}(C_9)$ and $\text{Im}(C_{10})$, the correlation between the integrated asymmetries $\langle A_7 \rangle$ and $\langle A_8 \rangle$ is completely different than that found in the FBMSSM (see the right-hand side plots in Figs. 8 and 12).

As a side comment, in our numerical analysis we have used the formulae of Ref. [64] modified by the additional term found in Ref. [66] which remove the UV cutoff dependent terms in C_9 and C_{10} . This modification decreases the two asymmetries by roughly a factor of 2 to 3. Whether this is the final result for the LHT model remains to be seen as the structure of the full heavy-fermion sector in the LHT model is rather involved and a complete analysis is still lacking.

6.3.4 General MSSM

Due to the huge number of free parameters in the general MSSM, a comprehensive analysis of this general framework is challenging. As a first step we therefore restrict ourselves to a framework in which NP effects are created dominantly by complex contributions to the Wilson coefficient C'_7 . Such a situation can easily be achieved in the general MSSM if one introduces flavour violating terms only in the left-right sector of the down squark mass. In particular, a $(\delta_d)_{32}^{LR}$ mass insertion will mostly create contributions to C'_7 by means of down squark – gluino loops, while at the same time leaving the other relevant Wilson coefficients SM like.

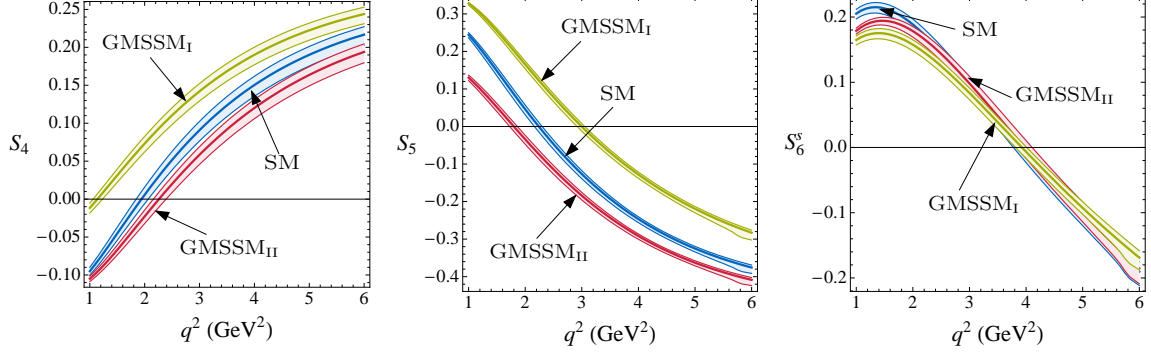


Figure 13: The observables S_4 , S_5 and S_6^s in the SM (blue band) and two GMSSM scenarios with large complex contributions to C_7' as described in the text.

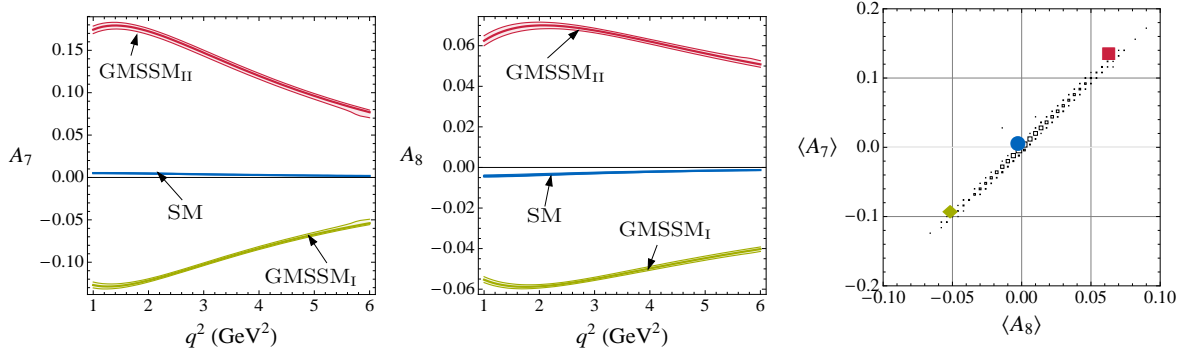


Figure 14: Left and centre plot: CP asymmetries A_7 and A_8 in the SM (blue band) and two general MSSM scenarios with large complex contributions to C_7' . Right plot: Correlation between the integrated asymmetries $\langle A_7 \rangle$ and $\langle A_8 \rangle$ in the framework of a general MSSM with large complex C_7' . The blue circle corresponds to the central SM value, while the green diamond represents scenario GMSSM_I and the red square scenario GMSSM_{II}.

Fig. 13 shows possible effects in S_4 , S_5 and S_6^s that arise in this framework due to the real part of C_7' , for two example scenarios, GMSSM_I and GMSSM_{II}. In Tab. 13, we collect the corresponding input parameters. Compared to the framework of the FBMSSM (see Fig. 9), the shift in the zeros of these observables show a completely different pattern. While the zero of S_6^s remains SM like, a positive shift in $q_0^2(S_4)$ implies a negative shift in $q_0^2(S_5)$ and vice versa.

Large imaginary parts of C_7' lead to sizeable effects in the asymmetries A_7 and A_8 , but again the pattern of these effects is different to that in the FBMSSM seen in Fig. 8. As shown in Fig. 14, a positive (negative) A_7 implies also a positive (negative) A_8 . In particular the correlation plot in the right panel of Fig. 14 is completely orthogonal to the one in the FBMSSM (see Fig. 8) and thus a clear distinction between these two frameworks is possible.

In addition a large complex C_7' also leads to large non-standard effects in the observables S_3 and A_9 as shown Fig. 15. In fact, as already mentioned in Sec. 6.2.1, effects in S_3 and A_9 are characteristic for scenarios with large NP contributions to the primed Wilson coefficients. The large effects in S_3 are driven by the real part of C_7' and directly correspond to the large effects in the transverse asymmetry $A_T^{(2)}$ that have been analysed in [44, 46, 21]. Having analysed possible effects in a particular non-minimal flavour violating MSSM framework we finally mention also the case of the general MSSM with generic flavour violating soft terms. Instead of presenting an exhaustive discussion of this framework, we concentrate on two specific scenarios that show effects that go beyond those discussed in the above.

Among the Wilson coefficients that are relevant in the decay $B \rightarrow K^* \mu^+ \mu^-$ the ones that are most sensitive to NP effects arising from flavour violating down squark masses are C_7 and C_7' . In the plots of Fig. 16 we show a scenario GMSSM_{IV} that corresponds to large NP contributions to both C_7 and C_7' . In contrast to the scenario with NP effects dominantly in C_7' discussed above, one observes e.g. sizeable effects in the zeros of S_5 and S_6^s while the zero in S_4 is much less affected.

One possibility to generate large effects in the Wilson coefficient C_{10} in a supersymmetric framework is through flavour violating entries in the left-right part of the up squark mass [72, 75, 78]. Scenario GMSSM_{III} in Fig. 16 corresponds exactly to such a scenario where in addition to large complex NP contributions to C_7 and C_7' , C_{10} also receives sizeable complex corrections through a $(\delta_u)_{32}^{LR}$ mass insertion. These curves show again a qualitatively different behaviour in various observables. For example large effects in S_3 and A_9 can be observed, that however do not show a zero in contrast to the red curves discussed above.

7 Summary and Conclusions

In this paper we have analysed all angular observables in the rare decay $B \rightarrow K^*(\rightarrow K\pi)\mu^+\mu^-$. They can be measured at the LHC and later at an upgraded Belle and a Super-B facility. These angular observables can be expressed in terms of CP-conserving and CP-violating quantities and offer new important tests of the SM and its extensions. To this end we have improved on previous studies in a number of ways that have been listed in Sec. 1.

Having identified angular observables with small to moderate dependence on hadronic quantities and large impact of NP we have analysed these observables first within the SM and subsequently within a number of its extensions like models with MFV, the flavour-blind MSSM with new flavour conserving, but CP-violating phases, the LHT model and also within a general MSSM with generic flavour violating soft terms.

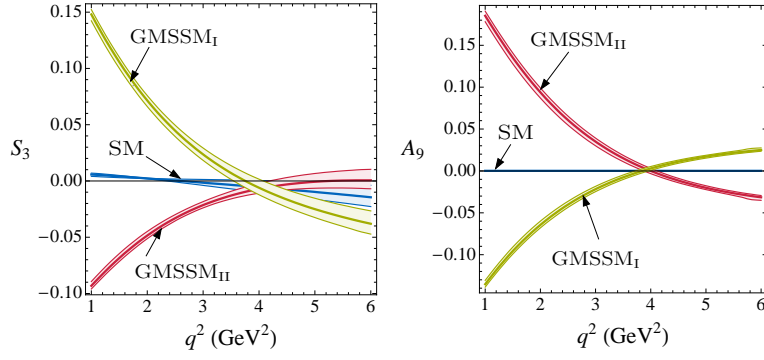


Figure 15: The observables S_3 and A_9 in the SM (blue band) and the two GMSSM scenarios GMSSM_{I,II} with large complex contributions to C'_7 as described in the text.

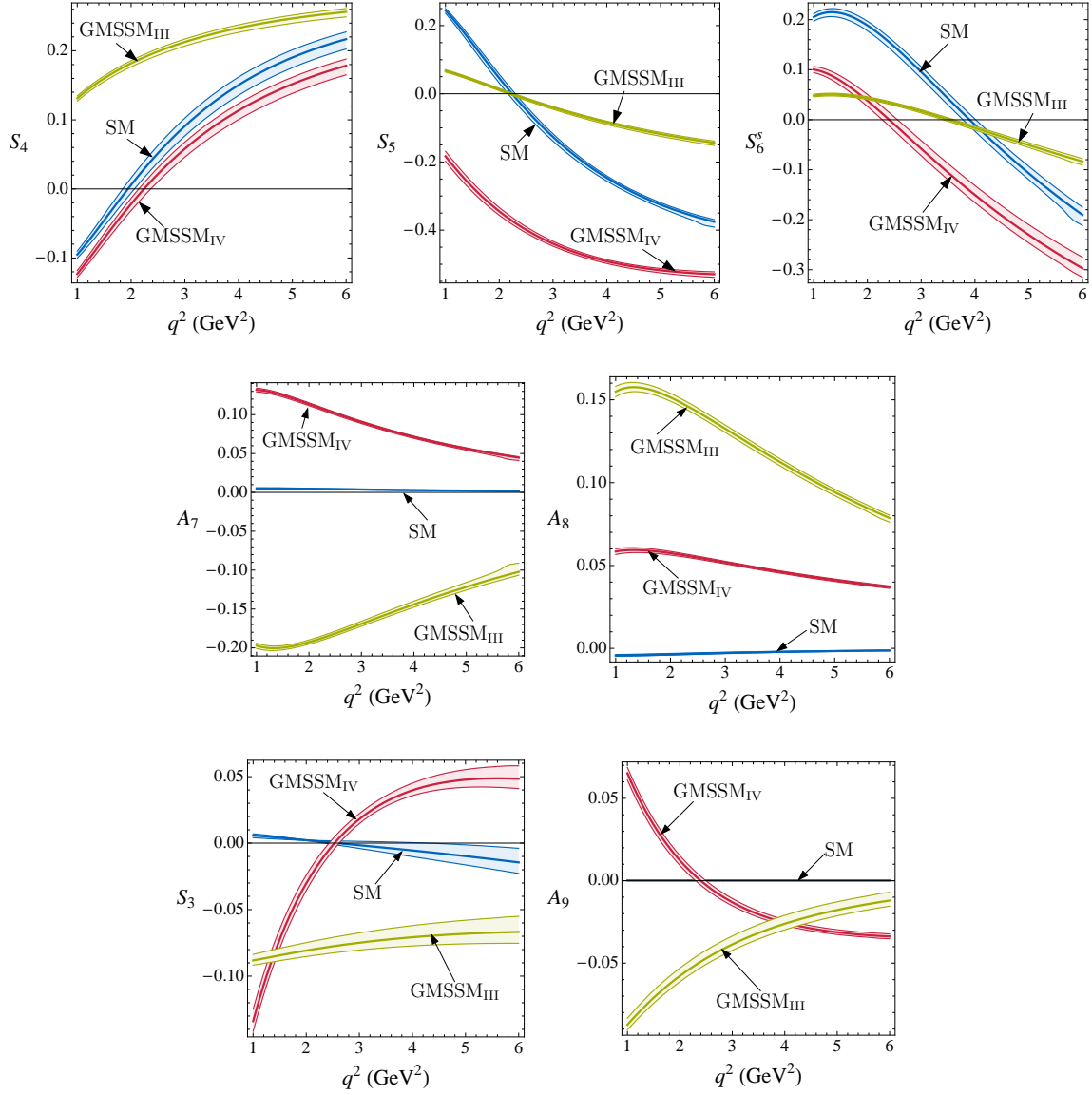


Figure 16: Several observables in the SM (blue band) and two selected GMSSM scenarios that show large non-standard behaviour. See text for details.

The main messages from this study are as follows:

- The most promising and complete set of observables in this channel are our $S_i^{(a)}$ and $A_i^{(a)}$ defined in Sec. 5.
- Our predictions for the CP-averaged angular coefficients $S_i^{(a)}$ in the SM are shown in Fig. 2. Some of these $S_i^{(a)}$ are found to be large.
- On the other hand, as evident from Fig. 3, the CP asymmetries $A_i^{(a)}$ are close to zero in the SM.
- Our model independent study shows that pseudoscalar operators are numerically irrelevant in the decay $B \rightarrow K^* \mu^+ \mu^-$. On the other hand a study of the angular distributions allows, in a way which is theoretically clean and complementary to $B_s \rightarrow \mu^+ \mu^-$, to probe the scalar sector of a theory beyond the SM.
- As one expects, the $A_i^{(a)}$ are SM like in MFV models. On the other hand, some of the $S_i^{(a)}$, in particular S_4 , S_5 and S_6^c can show deviations from the SM as seen in Figs. 6 and 7, where results in the MFV MSSM are shown.
- Probably the most interesting results are found in the FBMSSM, in which several $S_i^{(a)}$ and $A_i^{(a)}$ differ significantly, even by orders of magnitude from the SM results, and there exists a number of striking correlations among the observables discussed here and also correlations between A_7 (and A_8) and $A_{CP}(b \rightarrow s\gamma)$ and $S_{\phi K_S}$. All these results are shown in Figs. 8 to 11.
- In the LHT model only the CP asymmetries A_7 and A_8 differ significantly from the SM predictions, but these enhancements are smaller than found in the FBMSSM model. This different pattern of effects could easily distinguish these two models.
- As expected, in a general MSSM, the very large space of parameters does not allow for clear-cut conclusions. Almost all observables considered in the present paper can significantly differ from the SM results and the pattern of deviations can differ from those found in the FBMSSM and LHT models. This is illustrated in Figs. 13 to 16. This should allow these three models to be distinguished from each other.

Clearly, it will be very exciting to monitor the upcoming LHC, Belle upgrade and eventually Super-B factory in this and in the next decade to see whether the angular observables discussed in our paper will give a hint for any of the extensions of the SM.

Acknowledgements

The authors would like to thank S. Recksiegel for providing sets of input parameters for the Littlest Higgs model which are compatible with electroweak precision constraints, Th. Feldmann for several useful discussions and G. Hiller and C. Bobeth for clarifying communication. P.B. gratefully acknowledges financial support from the Cluster of Excellence ‘‘Origin and Structure of the Universe’’ at TU Munich. A.K.M.B. acknowledges receipt of a UK STFC studentship and financial support from Lehrstuhl T31, TU Munich. This work has been supported in part by the EU network contract No. MRTN-CT-2006-035482 (FLAVIANET), the

Appendices

A Kinematics of Four-Body Decays

In this appendix we collect some relevant results concerning the kinematics of the four-body decay $X \rightarrow Y(\rightarrow ab)Z(\rightarrow cd)$. For an excellent discussion see Ref. [84]. The translation of the general results to the notation appropriate for the decay $B \rightarrow K^*(\rightarrow K\pi)\mu^+\mu^-$ is given in Tab. A.

The four-body phase space is 4×4 -dimensional. The on-shell conditions of the final states reduce this number to 4×3 . Moreover, four-momentum conservation eliminates further 4 degrees of freedom. Eventually, exploiting isotropic symmetry, one can fix the three Euler angles and ends up with 5 physical degrees of freedom. It is customary and convenient to express them by the following set of variables, introduced first in Ref. [85] for the decay $K^+ \rightarrow \pi^+\pi^-e^+\nu$:

- m_{ab}^2 , the effective mass squared of the ab system, $m_a + m_b < m_{ab} < m_X - m_c - m_d$;
- m_{cd}^2 , the effective mass squared of the cd system, $m_c + m_d < m_{cd} < m_X - m_a - m_b$; note that $m_{ab} + m_{cd} < m_X$;
- θ_Y , the angle of the particle a in the c.m. system of the particles a and b with respect to the direction of flight of (a, b) in the Y rest system, $0 < \theta_Y < \pi$;
- θ_Z , the angle of the particle c in the c.m. system of the particles c and d with respect to the direction of flight of (c, d) in the Z rest system, $0 < \theta_Z < \pi$;
- θ_X , the angle between the plane formed by the decay products (a, b) in the X rest system and the corresponding plane of (c, d) , $-\pi < \theta_X < \pi$.

It is convenient to combine the four-momenta p_i , $i = a, b, c, d$, of the final-state particles into the following symmetric and antisymmetric momenta:

$$\begin{aligned} P_{ab} &= p_a + p_b, & Q_{ab} &= p_a - p_b, \\ P_{cd} &= p_c + p_d, & Q_{cd} &= p_c - p_d. \end{aligned}$$

The diparticle masses are then given by

$$P_{ab}^2 = m_{ab}^2, \quad P_{cd}^2 = m_{cd}^2.$$

Now we define the angles θ_X , θ_Y and θ_Z by

$$\cos \theta_Y = -\frac{\vec{Q}_{ab} \cdot \vec{P}_{cd}}{|\vec{Q}_{ab}| |\vec{P}_{cd}|}, \quad \cos \theta_Z = -\frac{\vec{Q}_{cd} \cdot \vec{P}_{ab}}{|\vec{Q}_{cd}| |\vec{P}_{ab}|}, \quad (\text{A.1})$$

$$\sin \theta_X = \frac{(\vec{P}_{ab} \times \vec{Q}_{ab}) \times (\vec{P}_{cd} \times \vec{Q}_{cd})}{|\vec{P}_{ab} \times \vec{Q}_{ab}| |\vec{P}_{cd} \times \vec{Q}_{cd}|}. \quad (\text{A.2})$$

It is important to note that the three-vectors in the above definition must be evaluated in the respective rest frames of the particles X , Y and Z .

With the above definitions, it is straightforward to express all remaining invariant products of the four-vectors P_{ab} , P_{cd} , Q_{ab} and Q_{cd} in terms of the five variables θ_X , θ_Y , θ_Z , m_{ab}^2 and m_{cd}^2 :

$$\begin{aligned} P_{ab}Q_{ab} &= m_a^2 - m_b^2, \\ P_{ab}P_{cd} &= \bar{p}, \\ P_{ab}Q_{cd} &= \frac{m_c^2 - m_d^2}{m_{cd}^2} \bar{p} + \frac{2}{m_{cd}^2} \sigma \sigma_{cd} \cos \theta_Z, \\ Q_{ab}Q_{ab} &= 2(m_a^2 + m_b^2) - m_{ab}^2, \\ Q_{ab}Q_{cd} &= \frac{1}{m_{ab}^2 m_{cd}^2} [(m_a^2 - m_b^2)(m_c^2 - m_d^2) \bar{p} \\ &\quad + 2\sigma \sigma_{ab} (m_c^2 - m_d^2) \cos \theta_Y \\ &\quad + 2\sigma \sigma_{cd} (m_a^2 - m_b^2) \cos \theta_Z \\ &\quad + 4\sigma_{ab} \sigma_{cd} \bar{p} \cos \theta_Y \cos \theta_Z \\ &\quad + 4\sigma_{ab} \sigma_{cd} m_{ab} m_{cd} \sin \theta_Y \sin \theta_Z \cos \theta_X], \\ \varepsilon_{\alpha\beta\gamma\delta} P_{ab}^\alpha Q_{ab}^\beta P_{cd}^\gamma Q_{cd}^\delta &= -\frac{4\sigma \sigma_{ab} \sigma_{cd}}{m_{cd} m_{ab}} \sin \theta_Y \sin \theta_Z \sin \theta_X. \end{aligned}$$

The remaining invariants can be obtained from the above by $(ab) \leftrightarrow (cd)$ and $\theta_Z \leftrightarrow \theta_Y$. Here we use

$$\begin{aligned} \bar{p} &= \frac{1}{2}(m_X^2 - m_{ab}^2 - m_{cd}^2), \\ \sigma &= \sqrt{\bar{p}^2 - m_{ab}^2 m_{cd}^2}, \\ \bar{p}_{ab} &= \frac{1}{2}(m_{ab}^2 - m_a^2 - m_b^2), \\ \sigma_{ab} &= \sqrt{\bar{p}_{ab}^2 - m_a^2 m_b^2} \end{aligned}$$

and corresponding expressions with $(ab) \rightarrow (cd)$. Tab. A provides the translation of the general notations introduced above to the special case $B \rightarrow K^*(\rightarrow K\pi)\mu^+\mu^-$.

general	$B \rightarrow K\pi\mu^+\mu^-$
(ab)	(πK)
(cd)	$(\mu^+\mu^-)$
m_{ab}	m_{K^*}
m_{cd}	$\sqrt{q^2}$
θ_X	ϕ
θ_Y	θ_{K^*}
θ_Z	θ_μ
σ_{ab}^2	$m_{K^*}^4\beta^2/4$
σ_{cd}^2	$q^4\beta_\mu^2/4$
σ^2	$\lambda^2/4$
\bar{p}	$(k \cdot q)$

Table A: Translation table between the variables of the general four-body decay $X \rightarrow Y(\rightarrow ab)Z(\rightarrow cd)$ discussed in App. A and the decay $B \rightarrow K^*(\rightarrow K\pi)\mu^+\mu^-$. Note that m_{ab} is fixed to m_{K^*} , which leads to an allowed range of q^2 of $(2m_\mu)^2 < q^2 < (m_B - m_{K^*})^2$. β , β_μ and λ are defined in Sec. 3.

B Form Factors and QCD Factorization

As we have seen in Sec. 2.3, the QCDF formulas for $B \rightarrow K^*\mu^+\mu^-$ are expressed in terms of two soft form factors $\xi_{\perp,\parallel}$, defined in Eqs. (2.25)–(2.26), rather than the seven form factors of Sec. 2.2, which implies certain relations between them, valid in the large energy limit. These relations are the topic of this appendix and we shall demonstrate that they are indeed fulfilled by light-cone sum rules (LCSRs) – both analytically and numerically.

Exploiting Eq. (2.28) for all 7 form factors, one can establish a number of relations which are expected to be valid for K^* energies $E \sim O(m_b)$ [11]:

$$\frac{A_1(q^2)}{V(q^2)} = \frac{2Em_B}{(m_B + m_{K^*})^2}, \quad (\text{B.1})$$

$$\frac{T_1(q^2)}{V(q^2)} = \frac{m_B}{2E} \frac{T_2(q^2)}{V(q^2)} = \frac{m_B}{m_B + m_{K^*}} \left(1 + \frac{\alpha_s C_F}{4\pi} \left[\ln \frac{m_b^2}{\mu^2} - L \right] + \frac{\alpha_s C_F}{4\pi} \frac{m_B}{4E} \frac{\Delta F_\perp}{\xi_\perp(q^2)} \right), \quad (\text{B.2})$$

$$\begin{aligned} & \frac{(m_B + m_{K^*})/(2E) A_1(q^2) - (m_B - m_{K^*})/m_B A_2(q^2)}{(m_{K^*}/E) A_0(q^2)} = \\ & 1 + \frac{\alpha_s C_F}{4\pi} [-2 + 2L] - \frac{\alpha_s C_F}{4\pi} \frac{m_B(m_B - 2E)}{(2E)^2} \frac{\Delta F_\parallel}{(E/m_{K^*}) \xi_\parallel(q^2)}, \quad (\text{B.3}) \end{aligned}$$

$$\frac{(m_B/2E) T_2(q^2) - T_3(q^2)}{(m_{K^*}/E) A_0(q^2)} = 1 + \frac{\alpha_s C_F}{4\pi} \left[\ln \frac{m_b^2}{\mu^2} - 2 + 4L \right] - \frac{\alpha_s C_F}{4\pi} \left(\frac{m_B}{2E} \right)^2 \frac{\Delta F_\parallel}{(E/m_{K^*}) \xi_\parallel(q^2)}, \quad (\text{B.4})$$

respectively. The abbreviations on the right hand side are defined as

$$\begin{aligned}
L &= -\frac{2E}{m_B - 2E} \ln \frac{2E}{m_B}, \\
\Delta F_\perp &= \frac{8\pi^2 f_B f_{K^*}^\perp}{3m_B} \frac{1}{\lambda_B} \int du \frac{\phi_\perp(u)}{1-u}, \\
\Delta F_\parallel &= \frac{8\pi^2 f_B f_{K^*}^\parallel}{3m_B} \frac{1}{\lambda_B} \int du \frac{\phi_\parallel(u)}{1-u}
\end{aligned} \tag{B.5}$$

in terms of the twist-2 K^* DAs $\phi_{\perp,\parallel}$ and the first inverse moment of the B meson DA, $1/\lambda_B$. E , the K^* 's energy, is related to q^2 by $2m_B E = m_B^2 - q^2$ (terms in $m_{K^*}^2$ are neglected). Numerical values of these parameters are given in Tab. 3.

One requirement for the LCSRs is obviously that they fulfill the above relations, to the required accuracy, i.e. in the large energy limit, and that the leading contributions to $\xi_{\perp(\parallel)}$ come from transversal (longitudinal) DAs. The above relations imply in particular that both A_1 and A_2 must to leading order be given in terms of transversal DAs, while these contributions must cancel in the combination $(m_B + m_{K^*})/(2E) A_1 - (m_B - m_{K^*})/m_B A_2$. As this is an important point, we write down the tree-level contributions to these sum rules, and that for V , explicitly ($\bar{u} = 1 - u$, $u_0 = (m_b^2 - q^2)/(s_0 - q^2)$):

$$\begin{aligned}
A_0(q^2) &= \frac{m_b}{m_B^2 f_B} e^{m_B^2/M^2} \left[\frac{f_{K^*}^\parallel m_b}{2} \int_{u_0}^1 du e^{-\frac{m_b^2 - \bar{u}q^2}{uM^2}} \frac{1}{u} \left[g_v(u) + \left\{ 1 + u \frac{d}{du} \right\} \left(\frac{\Phi(u)}{u} \right) \right] \right. \\
&\quad \left. + \dots \right], \tag{B.6}
\end{aligned}$$

$$\begin{aligned}
A_1(q^2) &= \frac{m_b e^{m_B^2/M^2}}{m_B^2 f_B (m_B + m_{K^*})} \int_{u_0}^1 du e^{-\frac{m_b^2 - \bar{u}q^2}{uM^2}} \frac{1}{u} \left[f_{K^*}^\perp (m_b^2 - q^2) \frac{\phi_\perp(u)}{2u} + f_{K^*}^\parallel m_b m_{K^*} g_v(u) \right. \\
&\quad \left. + \dots \right], \tag{B.7}
\end{aligned}$$

$$\begin{aligned}
A_2(q^2) &= \frac{m_b e^{m_B^2/M^2}}{m_B^2 f_B (m_B - m_{K^*})} \int_{u_0}^1 du e^{-\frac{m_b^2 - \bar{u}q^2}{uM^2}} \frac{1}{u} \left[f_{K^*}^\perp (m_b^2 - \bar{u}q^2) \frac{\phi_\perp(u)}{2u} \right. \\
&\quad \left. - f_{K^*}^\parallel m_b m_{K^*} \frac{m_b^2 - \bar{u}q^2}{m_b^2 - q^2} \left\{ 1 + u \frac{d}{du} \right\} \frac{\Phi(u)}{u} + \dots \right], \tag{B.8}
\end{aligned}$$

$$\begin{aligned}
V(q^2) &= \frac{m_B + m_{K^*}}{2} \frac{m_b e^{m_B^2/M^2}}{m_B^2 f_B} \int_{u_0}^1 du e^{-\frac{m_b^2 - \bar{u}q^2}{uM^2}} \frac{1}{u} \left[f_{K^*}^\perp \phi_\perp(u) \right. \\
&\quad \left. - \frac{u}{2(m_b^2 - q^2)} f_{K^*}^\parallel m_b m_{K^*} \frac{d}{du} g_a(u) + \dots \right]. \tag{B.9}
\end{aligned}$$

The dots stand for terms with higher powers of m_{K^*} . All DAs multiplying $f_{K^*}^{(\perp)}$ are longitudinal (transversal). Note that, as mentioned in Sec. 2.2, the suppression factor of higher-twist terms is given by $m_b m_{K^*}/(m_b^2 - q^2)$, which indicates the break-down of the expansion for $q^2 \rightarrow m_b^2$. Comparing the above formulas with (B.3) one finds that for $q^2 = 0$ ($E = m_B/2$) the terms in

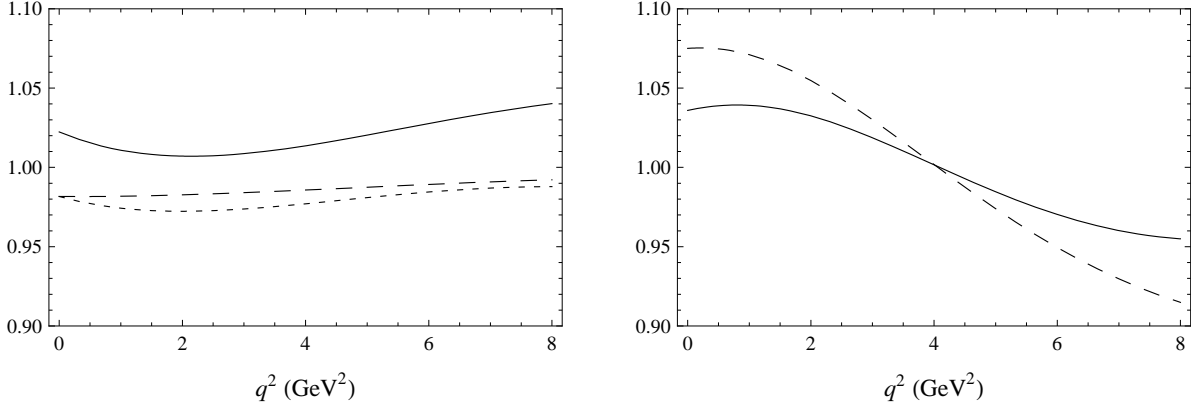


Figure A: Form factor ratios (B.1) to (B.4), l.h.s. divided by r.h.s., calculated from LCSRs with central values of input parameters. In the perfect heavy quark limit, all ratios equal 1. Left: form factor ratios based on ξ_\perp . Solid curve: (B.1), long dashes: (B.2) with T_1/V , short dashes: (B.2) with T_2/V . Right: form factor ratios based on ξ_\parallel . Solid curve: (B.3), long dashes: (B.4). α_s is evaluated at the scale $\mu^2 = m_B^2 - m_b^2 = O(m_b)$.

ϕ_\perp cancel exactly in the combination of A_1 and A_2 and (B.3) is reproduced up to terms in higher powers of m_{K^*} (which are neglected in the large energy limit). For $q^2 \neq 0$, however, there appears to be a non-vanishing term in $f_{K^*}^\perp$:

$$(m_B + m_{K^*})/(2E) A_1 - (m_B - m_{K^*})/m_B A_2 \sim \frac{m_b e^{m_B^2/M^2}}{m_B^2 f_B} \int_{u_0}^1 du e^{-\frac{m_b^2 - \bar{u}q^2}{uM^2}} f_{K^*}^\perp \frac{\phi_\perp(u)}{u} \frac{q^2(m_b^2 - q^2 - u(m_B^2 - q^2))}{2m_B(m_B^2 - q^2)u}. \quad (\text{B.10})$$

At this point it is useful to recall that, ideally, if the continuum model was perfect and all terms in the twist expansion were known, the LCSR would be independent of s_0 and M^2 . In reality, LCSRs are non-trivial functions of both parameters and the form factors are extracted within an interval of M^2 where the dependence on that parameter is small, i.e. the sum rules are evaluated near an extremum in M^2 , if such an extremum exists. In Ref. [86] we have argued that the central value of form factors should be evaluated exactly *at* the extremum. This implies that for both an ideal LCSR with completely known hadronic spectral density $\rho(u)$ and a realistic one with $\rho(u)$ known to a certain accuracy in the light-cone expansion one requires

$$\begin{aligned} \frac{d}{dM^2} \int_{u_0}^1 du e^{\frac{m_B^2}{M^2} - \frac{m_b^2 - \bar{u}q^2}{uM^2}} \rho(u) &= 0 \\ \longleftrightarrow \int_{u_0}^1 du e^{\frac{m_B^2}{M^2} - \frac{m_b^2 - \bar{u}q^2}{uM^2}} \frac{um_B^2 - m_b^2 + \bar{u}q^2}{u} \rho(u) &= 0. \end{aligned} \quad (\text{B.11})$$

As the integral must vanish, one finds that $\rho(u)$ effectively equals $(m_b^2 - q^2)/(m_B^2 - q^2) \rho(u)/u$ at and near the extremum. Hence the r.h.s. of (B.10) *vanishes* at the minimum in M^2 if the l.h.s. is treated as LCSR in its own right and not as sum of two different sum rules (with possibly different extrema in M^2 and different optimal values in s_0). This is also the reason why, in order to obtain values for $A_0(0)$ and ξ_\parallel , it is not useful to add the numbers for the individual form factors A_1 and A_2 obtained from LCSRs in Ref. [34]. Instead, the

above combination of A_1 and A_2 has to be evaluated anew. We would like to add that the cancellation of the contribution of ϕ_\perp to ξ_\parallel can also be made manifest by including the factor $1/E$ into the dispersion relation, using the above result that factors $um_B^2 - m_b^2 + \bar{u}q^2$ return zero under the integral if it is evaluated at the minimum in M^2 . One then can make the replacement

$$\frac{1}{2E} \rightarrow \frac{1}{m_B} \frac{m_b^2 - \bar{u}q^2}{m_b^2 - q^2}$$

upon which the contribution in ϕ_\perp cancels explicitly so that

$$\frac{m_B + m_{K^*}}{2E} A_1 - \frac{m_B - m_{K^*}}{m_B} A_2 = \frac{m_{K^*}}{E} A_0 + O(\alpha_s) + \dots$$

in the LCSR method. Again, the dots denote terms in higher powers of m_{K^*} . Similar analyses can be done for the other form factors ratios, for instance A_1/V , Eq. (B.1). Making again use of the fact that an additional factor u under the integral equals $(m_b^2 - q^2)/(m_B^2 - q^2)$, one finds from (B.7) and (B.9) that (B.1) is fulfilled to twist-2 accuracy, but also that the ratio deviates from the r.h.s. of (B.1) at twist-3 level, i.e. at $O(m_{K^*}/m_b)$.

Turning to the $O(\alpha_s)$ corrections in (B.1) to (B.4), we can confirm that to twist-2 accuracy (B.1) does not receive any such corrections: they cancel exactly between numerator and denominator. Reproducing the $O(\alpha_s)$ corrections in (B.2) to (B.4) is less trivial and requires to explicitly perform the limit $m_b \rightarrow \infty$ of the integral over u . We refrain from doing this analysis explicitly, but refer to Ref. [87] where it was shown, for $B \rightarrow \pi$ transitions, that LCSRs fulfill the SCET relations also at $O(\alpha_s)$.

In Fig. A we plot the form factor ratios as functions of q^2 for central values of the input parameters, separately for ratios based on ξ_\perp and those based on ξ_\parallel . All ratios include the $O(\alpha_s)$ corrections calculated in QCDF. We find that, overall, the QCDF predictions are fulfilled by the full QCDF form factors from LCSRs at the level of 10% or better. Nonetheless there is a considerable dependence of the ξ_\parallel ratios on q^2 . This is due to $1/m_b$ corrections which are neglected in QCDF, but turn out to be, numerically, larger than the factorizable $O(\alpha_s)$ corrections calculable in QCDF. As a consequence, we expect that the transversity amplitudes $A_{\perp(\parallel)L,R}$ of Sec. 3.2, and all angular observables built from them, should be rather insensitive to $1/m_b$ corrections, i.e. corrections to QCDF, while $A_{0L,R}$, A_t , A_S and all corresponding angular variables will be affected by such corrections to a larger degree.

References

- [1] T. Hurth, Int. J. Mod. Phys. A **22** (2007) 1781 [arXiv:hep-ph/0703226].
- [2] R. Ammar *et al.* [CLEO Collaboration], Phys. Rev. Lett. **71** (1993) 674.
- [3] J. R. Ellis *et al.*, JHEP **0708** (2007) 083 [arXiv:0706.0652 [hep-ph]].
- [4] P. Ball and R. Zwicky, Phys. Lett. B **642** (2006) 478 [arXiv:hep-ph/0609037].
- [5] F. Krüger, L. M. Sehgal, N. Sinha and R. Sinha, Phys. Rev. D **61** (2000) 114028 [Erratum-ibid. D **63** (2001) 019901] [arXiv:hep-ph/9907386].
- [6] B. Aubert *et al.* [BABAR Collaboration], arXiv:0804.4412 [hep-ex].

- [7] J.-T. Wei, talk at ICHEP 2008.
- [8] G. Eigen, arXiv:0807.4076 [hep-ex].
- [9] T. Aaltonen *et al.* [CDF Collaboration], arXiv:0804.3908 [hep-ex].
- [10] J. Dickens, V. Gibson, C. Lazzeroni and M. Patel, LHCb note CERN-LHCB-2007-039.
- [11] M. Beneke and T. Feldmann, Nucl. Phys. B **592** (2001) 3 [arXiv:hep-ph/0008255].
- [12] M. Beneke, T. Feldmann and D. Seidel, Nucl. Phys. B **612** (2001) 25 [arXiv:hep-ph/0106067].
- [13] M. Beneke, T. Feldmann and D. Seidel, Eur. Phys. J. C **41** (2005) 173 [arXiv:hep-ph/0412400].
- [14] P. Colangelo and A. Khodjamirian, hep-ph/0010175;
A. Khodjamirian, AIP Conf. Proc. **602** (2001) 194 [arXiv:hep-ph/0108205].
- [15] G. Hiller and F. Krüger, Phys. Rev. D **69** (2004) 074020 [arXiv:hep-ph/0310219].
- [16] A. Ali, P. Ball, L. T. Handoko and G. Hiller, Phys. Rev. D **61** (2000) 074024 [arXiv:hep-ph/9910221].
- [17] T. Feldmann and J. Matias, JHEP **0301** (2003) 074 [arXiv:hep-ph/0212158].
- [18] B. Aubert *et al.* [BABAR Collaboration], arXiv:0807.4119 [hep-ex].
- [19] A. Ali, G. Kramer and G. H. Zhu, Eur. Phys. J. C **47** (2006) 625 [arXiv:hep-ph/0601034].
- [20] C. Bobeth, G. Hiller and G. Piranishvili, JHEP **0807** (2008) 106 [arXiv:0805.2525 [hep-ph]].
- [21] U. Egede *et al.*, arXiv:0807.2589 [hep-ph].
- [22] C. S. Kim and T. Yoshikawa, arXiv:0711.3880 [hep-ph].
- [23] C. Bobeth, M. Misiak and J. Urban, Nucl. Phys. B **574** (2000) 291 [arXiv:hep-ph/9910220].
- [24] C. Bobeth, A. J. Buras, F. Krüger and J. Urban, Nucl. Phys. B **630** (2002) 87 [arXiv:hep-ph/0112305].
- [25] P. Gambino, M. Gorbahn and U. Haisch, Nucl. Phys. B **673** (2003) 238 [arXiv:hep-ph/0306079].
- [26] M. Gorbahn and U. Haisch, Nucl. Phys. B **713** (2005) 291 [arXiv:hep-ph/0411071];
M. Gorbahn, U. Haisch and M. Misiak, Phys. Rev. Lett. **95** (2005) 102004 [arXiv:hep-ph/0504194].
- [27] C. Amsler *et al.* [Particle Data Group], Phys. Lett. B **667** (2008) 1.
- [28] The Tevatron Electroweak Working Group, arXiv:0808.1089 [hep-ex].

- [29] A. J. Buras, M. Misiak, M. Münz and S. Pokorski, Nucl. Phys. B **424** (1994) 374 [arXiv:hep-ph/9311345].
- [30] D. Becirevic, V. Lubicz and F. Mescia, Nucl. Phys. B **769** (2007) 31 [arXiv:hep-ph/0611295].
- [31] S. Meinel *et al.*, PoS **LAT2007** (2007) 377 [arXiv:0710.3101 [hep-lat]].
- [32] V. L. Chernyak and A. R. Zhitnitsky, JETP Lett. **25** (1977) 510 [Pisma Zh. Eksp. Teor. Fiz. **25** (1977) 544]; Sov. J. Nucl. Phys. **31** (1980) 544 [Yad. Fiz. **31** (1980) 1053]; A.V. Efremov and A.V. Radyushkin, Phys. Lett. B **94** (1980) 245; Theor. Math. Phys. **42** (1980) 97 [Teor. Mat. Fiz. **42** (1980) 147]; G.P. Lepage and S.J. Brodsky, Phys. Lett. B **87** (1979) 359; Phys. Rev. D **22** (1980) 2157; V.L. Chernyak, A.R. Zhitnitsky and V.G. Serbo, JETP Lett. **26** (1977) 594 [Pisma Zh. Eksp. Teor. Fiz. **26** (1977) 760]; Sov. J. Nucl. Phys. **31** (1980) 552 [Yad. Fiz. **31** (1980) 1069].
- [33] P. Ball and V. M. Braun, Phys. Rev. D **58** (1998) 094016 [arXiv:hep-ph/9805422].
- [34] P. Ball and R. Zwicky, Phys. Rev. D **71** (2005) 014029 [arXiv:hep-ph/0412079].
- [35] M.A. Shifman, A.I. Vainshtein and V.I. Zakharov, Nucl. Phys. B **147** (1979) 385; Nucl. Phys. B **147** (1979) 448.
- [36] P. Ball and R. Zwicky, JHEP **0604** (2006) 046 [arXiv:hep-ph/0603232].
- [37] P. Ball and R. Zwicky, Phys. Lett. B **633** (2006) 289 [arXiv:hep-ph/0510338]; JHEP **0602** (2006) 034 [arXiv:hep-ph/0601086]; P. Ball and G. W. Jones, JHEP **0703** (2007) 069 [arXiv:hep-ph/0702100]; P. Ball, V. M. Braun and A. Lenz, JHEP **0708** (2007) 090 [arXiv:0707.1201 [hep-ph]].
- [38] A. Khodjamirian *et al.*, Phys. Rev. D **62** (2000) 114002 [arXiv:hep-ph/0001297]; P. Ball, Phys. Lett. B **641** (2006) 50 [arXiv:hep-ph/0608116].
- [39] T. Onogi, PoS **LAT2006** (2006) 017 [arXiv:hep-lat/0610115].
- [40] M. Steinhauser, arXiv:0809.1925 [hep-ph].
- [41] P. Ball, G. W. Jones and R. Zwicky, Phys. Rev. D **75** (2007) 054004 [arXiv:hep-ph/0612081].
- [42] S. J. Brodsky and G. P. Lepage, Adv. Ser. Direct. High Energy Phys. **5** (1989) 93.
- [43] C. S. Kim, Y. G. Kim, C. D. Lu and T. Morozumi, Phys. Rev. D **62** (2000) 034013 [arXiv:hep-ph/0001151].
- [44] F. Krüger and J. Matias, Phys. Rev. D **71** (2005) 094009 [arXiv:hep-ph/0502060].
- [45] A. Faessler, T. Gutsche, M. A. Ivanov, J. G. Körner and V. E. Lyubovitskij, Eur. Phys. J. direct C **4** (2002) 18 [arXiv:hep-ph/0205287].
- [46] E. Lunghi and J. Matias, JHEP **0704** (2007) 058 [arXiv:hep-ph/0612166].

- [47] D. Seidel, Phys. Rev. D **70** (2004) 094038 [arXiv:hep-ph/0403185].
- [48] J. A. Ellison [D0 Collaboration], arXiv:0810.1041 [hep-ex];
D. Tonelli [CDF Collaboration], arXiv:0810.3229 [hep-ex].
- [49] A. J. Buras *et al.*, Phys. Lett. B **500** (2001) 161 [arXiv:hep-ph/0007085].
- [50] A. J. Buras, Acta Phys. Polon. B **34** (2003) 5615 [arXiv:hep-ph/0310208].
- [51] M. Blanke, A. J. Buras, D. Guadagnoli and C. Tarantino, JHEP **0610** (2006) 003 [arXiv:hep-ph/0604057].
- [52] C. Bobeth *et al.*, Nucl. Phys. B **726** (2005) 252 [arXiv:hep-ph/0505110].
- [53] U. Haisch and A. Weiler, Phys. Rev. D **76** (2007) 074027 [arXiv:0706.2054 [hep-ph]].
- [54] G. D'Ambrosio, G. F. Giudice, G. Isidori and A. Strumia, Nucl. Phys. B **645** (2002) 155 [arXiv:hep-ph/0207036].
- [55] S. Baek and P. Ko, Phys. Rev. Lett. **83** (1999) 488 [arXiv:hep-ph/9812229]; Phys. Lett. B **462** (1999) 95 [arXiv:hep-ph/9904283].
- [56] A. Bartl *et al.* Phys. Rev. D **64** (2001) 076009 [arXiv:hep-ph/0103324].
- [57] J. R. Ellis, J. S. Lee and A. Pilaftsis, Phys. Rev. D **76** (2007) 115011 [arXiv:0708.2079 [hep-ph]].
- [58] W. Altmannshofer, A. J. Buras and P. Paradisi, arXiv:0808.0707 [hep-ph].
- [59] H. C. Cheng and I. Low, JHEP **0309** (2003) 051 [arXiv:hep-ph/0308199].
- [60] H. C. Cheng and I. Low, JHEP **0408** (2004) 061 [arXiv:hep-ph/0405243].
- [61] J. Hubisz, S. J. Lee and G. Paz, JHEP **0606** (2006) 041 [arXiv:hep-ph/0512169].
- [62] M. Blanke *et al.*, Phys. Lett. B **646** (2007) 253 [arXiv:hep-ph/0609284].
- [63] M. Blanke *et al.*, JHEP **0612** (2006) 003 [arXiv:hep-ph/0605214].
- [64] M. Blanke *et al.*, JHEP **0701** (2007) 066 [arXiv:hep-ph/0610298].
- [65] M. Blanke *et al.*, JHEP **0705** (2007) 013 [arXiv:hep-ph/0702136].
- [66] T. Goto, Y. Okada and Y. Yamamoto, arXiv:0809.4753 [hep-ph].
- [67] M. Blanke, A. J. Buras, S. Recksiegel and C. Tarantino, arXiv:0805.4393 [hep-ph].
- [68] F. Gabbiani, E. Gabrielli, A. Masiero and L. Silvestrini, Nucl. Phys. B **477** (1996) 321 [arXiv:hep-ph/9604387].
- [69] T. Besmer, C. Greub and T. Hurth, Nucl. Phys. B **609** (2001) 359 [arXiv:hep-ph/0105292].
- [70] M. Ciuchini, E. Franco, A. Masiero and L. Silvestrini, Phys. Rev. D **67** (2003) 075016 [Erratum-ibid. D **68** (2003) 079901] [arXiv:hep-ph/0212397].

- [71] J. Foster, K. I. Okumura and L. Roszkowski, JHEP **0508** (2005) 094 [arXiv:hep-ph/0506146]; Phys. Lett. B **641** (2006) 452 [arXiv:hep-ph/0604121].
- [72] E. Lunghi, A. Masiero, I. Scimemi and L. Silvestrini, Nucl. Phys. B **568** (2000) 120 [arXiv:hep-ph/9906286].
- [73] E. Gabrielli and S. Khalil, Phys. Lett. B **530** (2002) 133 [arXiv:hep-ph/0201049].
- [74] E. Lunghi and I. Scimemi, Nucl. Phys. B **574** (2000) 43 [arXiv:hep-ph/9912430].
- [75] G. Buchalla, G. Hiller and G. Isidori, Phys. Rev. D **63** (2001) 014015 [arXiv:hep-ph/0006136].
- [76] T. Aaltonen *et al.* [CDF Collaboration], Phys. Rev. Lett. **100** (2008) 101802 [arXiv:0712.1708 [hep-ex]].
- [77] T. Hurth, G. Isidori, J. F. Kamenik and F. Mescia, arXiv:0807.5039 [hep-ph].
- [78] A. Ali, E. Lunghi, C. Greub and G. Hiller, Phys. Rev. D **66** (2002) 034002 [arXiv:hep-ph/0112300].
- [79] P. Gambino, U. Haisch and M. Misiak, Phys. Rev. Lett. **94** (2005) 061803 [arXiv:hep-ph/0410155].
- [80] A. J. Buras, A. Poschenrieder, M. Spranger and A. Weiler, Nucl. Phys. B **678** (2004) 455 [arXiv:hep-ph/0306158].
- [81] C. Bobeth, A. J. Buras and T. Ewerth, Nucl. Phys. B **713** (2005) 522 [arXiv:hep-ph/0409293].
- [82] E. Barberio *et al.* [Heavy Flavor Averaging Group], arXiv:0808.1297 [hep-ex], and online update at <http://www.slac.stanford.edu/xorg/hfag>.
- [83] B. C. Regan, E. D. Commins, C. J. Schmidt and D. DeMille, Phys. Rev. Lett. **88** (2002) 071805.
- [84] L. Widhalm, PhD. Thesis, TU Wien, 2001
- [85] N. Cabibbo and A. Maksymowicz, Phys. Rev. B **137** (1965) 438.
- [86] P. Ball and R. Zwicky, Phys. Rev. D **71** (2005) 014015 [arXiv:hep-ph/0406232].
- [87] P. Ball, arXiv:hep-ph/0308249.